

UNIVERSITY OF TARTU
Faculty of Science and Technology
Institute of Physics

Kamarniso Vrandecic

**Energy level structure and protein dynamics
in the light-harvesting complex II**

Master's thesis

Supervisor: Prof. Jörg Pieper

Tartu 2013

Table of Contents

Abstract	4
List of abbreviations	5
1. Photosynthesis	6
1.1. Light-harvesting complex II (LHC II)	8
1.2. Spectroscopic properties of LHC II	10
1.3. Literature data	11
2. Materials and methods	15
2.1. Lineshape of absorption bands.....	15
2.1.1. Homogeneous and inhomogeneous broadening.....	15
2.1.2. Electron-phonon coupling	16
2.2. Quasielastic neutron scattering (QENS).....	18
2.3. Sample preparation and measurements.....	24
2.3.1. Preparation of the LHC II mutants.....	24
2.3.2. Optical measurements of the LHC II mutants.....	25
2.3.3. QENS measurements of native LHC II	25
3. Experimental results	26
3.1. Optical experimental data about the LHC II mutants	26
3.1.1. Absorption and fluorescence spectra of the LHC II mutants at 4.5 K	26
3.1.2. Absorption difference spectra of the LHC II mutants	29
3.1.3. Maximum and full width at half maximum (FWHM) values of the absorption difference spectra of the LHC II mutants	32
3.2. Simulated fits of the LHC II mutants Chl <i>a</i> 612 and Chl <i>b</i> 606 absorption difference bands at 4.5 K.....	35
3.3. Quasielastic neutron scattering experimental data about native LHC II.....	38

4. Discussion	41
4.1. Electron-phonon coupling in LHC II.....	41
4.1.1. Simulated fits of the LHC II mutants Chl <i>a</i> 612 and Chl <i>b</i> 606 absorption difference bands at 4.5 K.....	41
4.1.2. Linear fits of the FWHM values of the three LHC II mutants.....	41
4.1.3. Table of the obtained S-factors for the LHC II mutants.....	46
4.2. The role of the LHC II mutant Chl <i>a</i> 612 for LHC II fluorescence at the temperature range from 4.5 K to 290 K.....	46
4.3. Temperature shift in the absorption difference spectra of the LHC II mutants Chl <i>a</i> 610, Chl <i>a</i> 612 and Chl <i>b</i> 606. Comparison with the protein dynamics of the native LHC II complex	48
4.4. Potential energy diagram	50
4.5. Conclusions about the LHC II mutants Chl <i>a</i> 610 and Chl <i>b</i> 606.....	51
5. Summary	52
6. Summary in Estonian / Kokkuvõte	54
Acknowledgements	56
References	57

Abstract

Light-harvesting complexes of plants play an important role in photosynthesis. They harvest solar energy and transfer it to the reaction center of a photosystem, where the energy conversion reactions are executed. Energy transfer to the reaction center happens due to complex pigment-pigment and pigment-protein interactions. Light-harvesting complex II (LHC II) is the most widespread antenna pigment-protein complex. The main goal of this thesis is to analyze the effects of pigment-pigment interactions and protein dynamics at low and elevated temperatures by combining optical spectroscopy and quasielastic neutron scattering methods.

During the data analysis, spectral positions and lineshapes of three chlorophyll molecules have been determined from absorption difference spectra of mutants lacking these chlorophylls in the temperature range of 4.5 K–290 K. It has been ascertained that Chl *a*612 contributes to fluorescence at all temperatures, but above 150 K, Chl *a*612 becomes the main contributor. The spectral position of the Chl *a*612 absorption band at ~677 nm exhibit a pronounced temperature dependence above 77 K all the way up to 680 nm.

The temperature dependent shift appears to be correlated with thermally activated protein motions between different conformational substates that are thermally accessible above 77 K. Chl *a*610 has a three peak structure in the absorption spectrum with peaks at ~670, ~672 and ~675 nm, because it is located in an excitonically coupled Chl *a* trimer. Chl *b*606 has a peak in the absorption band at ~648 nm. A fit of the absorption band reveals a Lorentzian lifetime broadening corresponding to a lifetime of 66 femtoseconds due to energy transfer.

Huang-Rhys-factors *S* characterizing electron-phonon coupling have been obtained from the analysis of the linewidths of absorption difference spectra of mutants in the three temperature ranges. The *S*-factors obtained are for Chl *a*612 0.44 at 4.5–60 K, 0.91 at 77–211 K, and 1.74 at 211–290 K; for Chl *a*610 0.45, 1.31, 1.05; and for Chl *b*606 0.47, 0.94, 1.82, respectively.

The thermal activation of conformational protein dynamics has been investigated independently by quasielastic neutron scattering. The data reveal three different temperature ranges with distinct protein dynamics: i) below 77 K, conformational protein motions are frozen, ii) in the 77–240 K temperature range, protein motions are partly thermally activated, and iii) with the dynamical transition at 240 K, there is a further activation of protein motions. Protein motions in these three temperature ranges differ in the magnitude of their dynamics. The coincidence of the temperature ranges with different protein dynamics with those exhibiting different spectroscopic properties like spectral position of absorption bands, linewidth and Huang-Rhys-factor *S* suggests a correlation of these effects. A potential model explaining these effects is presented.

List of abbreviations

Chl	chlorophyll
E. coli	escherichia coli
EET	excitation energy transfer
EISF	elastic incoherent structure factor
fs	femtosecond
FWHM	full width at half-maximum
HB	hole-burning
HPLC	high-performance liquid chromatography
INS	inelastic neutron scattering
LHC II	light harvesting complex II
NPHB	nonphotochemical hole-burning
ps	picosecond
PS I	photosystem I
PS II	photosystem II
PSB	phonon sideband
QENS	quasielastic neutron scattering
QISF	quasielastic incoherent structure factor
r.h.	relative hydration
SHB	spectral hole-burning
Xan	xanthophyll
ZPL	zero-phonon line

1. Photosynthesis

Photosynthesis is a process which plants, algae, and cyanobacteria use for transforming light energy into chemical energy. This process removes carbon dioxide from and releases oxygen molecules into the atmosphere [1].

The common equation for photosynthesis is:



Green plants have a photosynthetic apparatus situated in organelles called chloroplasts. Every chloroplast is comprised of stroma surrounded by a double-layer membrane. Thylakoids are sub-organelles laid over stroma and organized into grana (Figure 1).

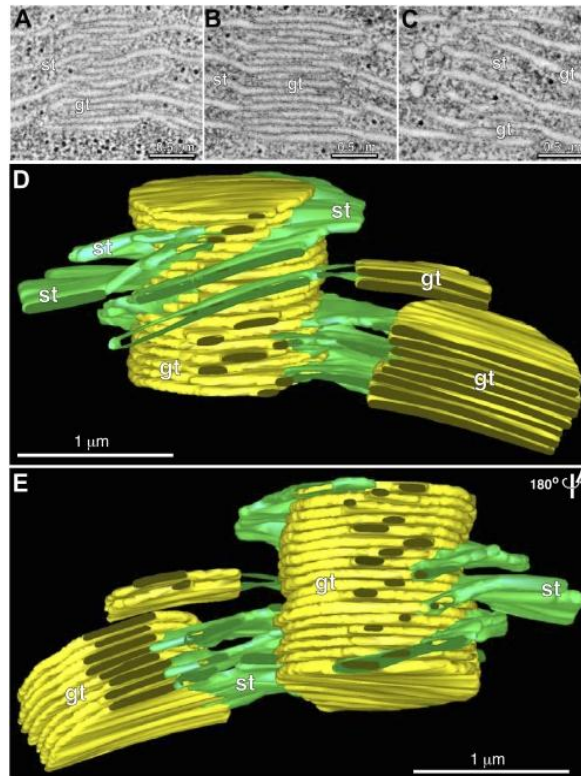


Figure 1: Stroma and grana thylakoid organization.

Tomographic slice images of grana thylakoids: A) front, B) middle, C) back.

Tomographic reconstructed models of grana thylakoids (yellow) and stroma thylakoids (green): D) front view, E) back view (rotated 180°) [2]. *Permission obtained.*

The thylakoids are the site where light reactions of photosynthesis take place. All chloroplasts have pigments, and the main pigment of chloroplasts of green plants is chlorophyll (Chl), which participates in oxygenic photosynthesis in two different forms — Chl *a* and *b*. Chlorophylls are IV-pyrrol ring molecules with one magnesium atom in the middle (Figure 2). The molecular formula for Chl *a* is $C_{55}H_{72}O_5N_4Mg$ and for Chl *b* $C_{55}H_{70}O_6N_4Mg$. These chlorophyll pigments can absorb the red, blue and violet portions of visible light very well. Plants appear green, because green light is absorbed only minimally by the pigments [3].

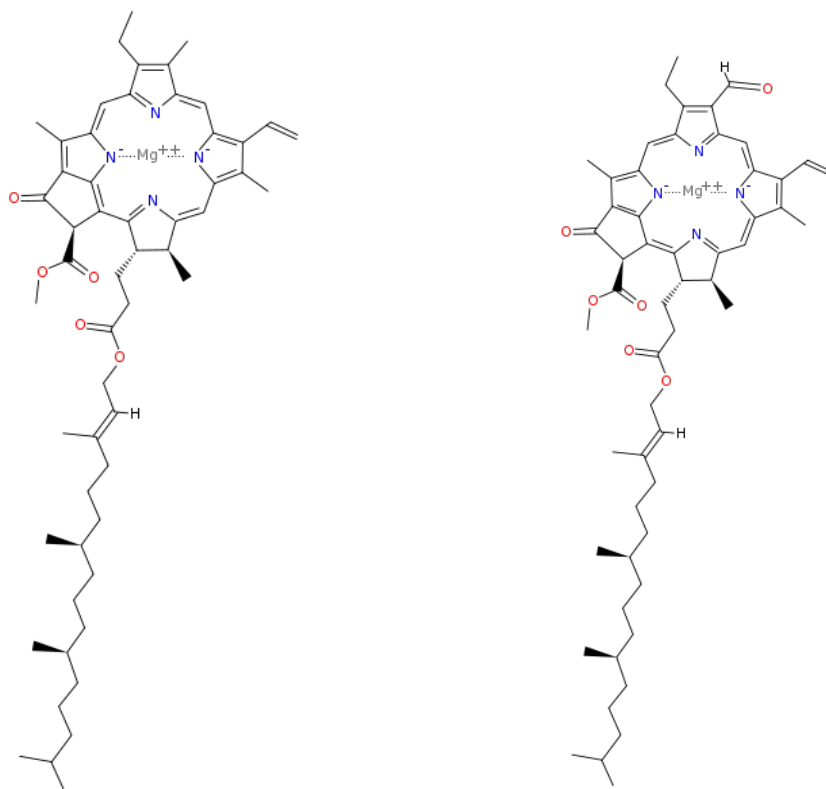


Figure 2: Chemical structures of Chl *a* (left) and Chl *b* (right) [4].

The main working units of photosynthesis are photosystems (PS) I and II. PS I is named so because it has been discovered before PS II, but the names are not related to the function of the photosystems.

Photosystems consist of the reaction center and light-harvesting antenna complexes. The reaction center can be viewed as an enzyme that catalyzes the light-driven reaction of photosynthesis. The light-harvesting antenna complexes (primarily LHC I for PS I and LHC II for PS II) absorb and transfer the light energy to the reaction centers (RC I and RC II respectively) [5].

The antenna system of PS II is built out of the core antenna, which is located close to the reaction center, minor antenna complexes and the major light-harvesting complex II, which is located peripherally. The core antenna consists of two pigment-protein complexes named CP47 and CP43 that bind Chl *a*. On the other hand, LHC II can bind Chl *a*, Chl *b* and xanthophylls. The peripheral antenna system of PS II is comprised of six pigment-protein complexes that bind Chl *a/b* denoted as Lhcb 1-6. The major light harvesting complex LHC II is constituted by Lhcb 1-3, whereas Lhcb 4-6 make up the minor antenna complexes — CP24, CP26 and CP29 [6].

Light-harvesting antenna complexes enhance spectral and spatial cross section of energy absorbed from the sun, and so ensure efficient light absorption also in low light [5].

The major LHC II will be described in the next section.

1.1. Light harvesting complex II (LHC II)

LHC II is the most widespread antenna pigment-protein complex situated in the thylakoid membrane, and it works as an antenna for the light harvesting in green plants. It is a chlorophyll-protein complex that transfers light energy to the Reaction Center of a photosystem. LHC II binds about 65% of the chlorophylls of PS II [7].

LHC II distributes the light energy absorbed in photosynthesis between the two photosystems [8]. In nature, LHC II occurs in trimeric form, and each monomer contains 13-15 Chl molecules, 3-4 carotenoids, and one phospholipid [7].

The monomers of LHC II are small proteins — approximately 25-28 kDa, containing alpha-helical structures. Electron microscopy and crystallography methods revealed the structure of the trimeric LHC II of pea with a resolution of 3.4Å in 1994 [9]. Later in 2004 and 2005, a higher resolution structural model of LHC II has been obtained almost simultaneously by Chinese [7] and German [10] research groups.

The chlorophylls in LHC II are arranged in the way that is the most efficient for light-harvesting. According to their orientation within the thylakoid membrane, chlorophylls in LHC II are distributed in two layers — one layer close to the stromal side, another one close to the luminal side (Figure 3a).

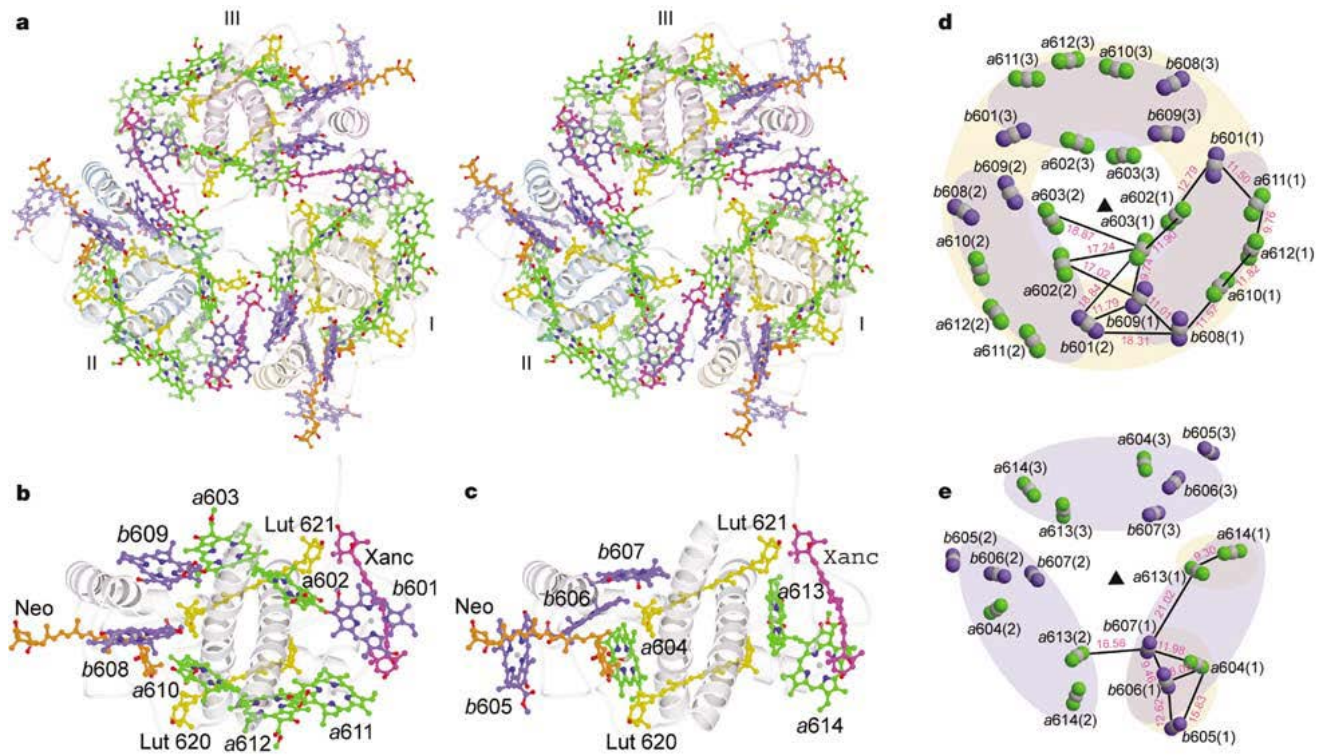


Figure 3: Arrangements of pigments in monomer and trimer LHC II.

a. Stereo view of the LHC II trimer. Roman numbers I, II, and III stand for LHC II monomers. Green – Chl *a*; blue – Chl *b*; yellow – lutein; orange – neoxanthin; magenta – xanthophylls; **b.** Pigment pattern in the LHC II monomer (stromal side); **c.** Pigment pattern in the LHC II monomer (luminal side); **d.** Pigment arrangement in the LHC II trimer (stromal side); **e.** Pigment arrangement in the LHC II trimer (luminal side). Chlorophylls are shown as three atoms – a magnesium atom in the center surrounded by two atoms of nitrogen. Numerical notes in magenta between two chlorophylls show the distance from one center to the other in Å [7]. *Permission obtained.*

LHC II is one of the best studied pigment-protein complexes, because the purification process of LHC II (i.e., its isolation from thylakoids) was very well developed since 1988 [11].

1.2. Spectroscopic properties of LHC II.

LHC II has been a focus of many spectroscopic studies because of the availability of its structural model. Nonetheless, there are still unanswered questions related to its excited state energy level structure and EET. The major question regarding the spectroscopic properties of LHC II is the relation between its structure and light-harvesting function.

The absorption and fluorescence spectra of the LHC II trimer measured at temperature 4.2 K is given in Figure 4 below.

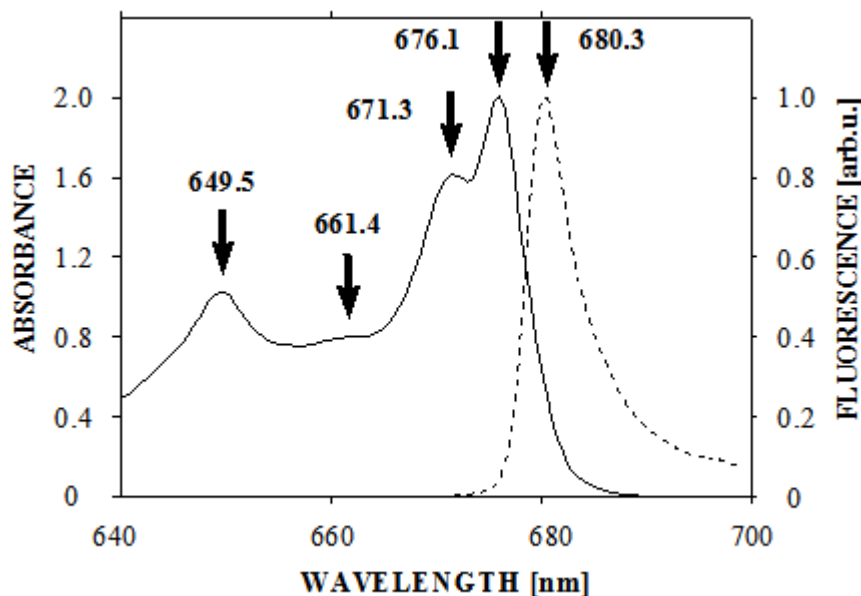


Figure 4: Q_y -absorption and fluorescence spectra of trimeric LHC II at low temperature (4.2 K) [6].
Permission obtained.

The four arrows in the Q_y -absorption region in Figure 4 label the few characteristic peaks in the Q_y absorption spectrum of LHC II. The further substructure is hidden: we cannot see absorption bands for all 42 Chl of LHC II, and thus no structural assignment is possible.

According to previous studies [12], Chl *b* is responsible for the absorption at the ~650 nm wavelength, and the absorption at the ~670-680 nm wavelength happens due to Chl *a*.

The Q_y -absorption spectrum is not established only because of the superpositions of Chl molecules in the LHC II. Pigment-pigment-, pigment-protein-, and pigment-vibration-interactions determine the shape of the absorption spectrum of the LHC II pigments.

Chl-Chl interaction: Excited pigment molecules can be considered as an oscillating dipole. This oscillation might be represented as a perturbation to the neighboring ground state pigment

molecule. Due to this perturbation there is a chance that when the first molecule returns into its ground state, the second molecule becomes excited. This kind of collective excitation is called *exciton*. The strength of Chl-Chl interaction depends on the center-to-center distance, and the mutual orientation of the dipole moments of the interacting pigments [6].

Chl-protein interaction: Pigment molecules in LHC II are connected to the protein with hydrogen or ligation bonds. These bonding interactions might represent a perturbation of electronic transitions, and hence, lead to the absorption frequency shift at certain chlorophyll binding sites. Moreover, the inherent heterogeneity of the protein environment may cause inhomogeneous broadening (see Section 2.1.1).

Chl-vibration interaction: The homogeneously broadened absorption spectrum is composed of an electronic transition accompanied with vibrational satellites due to pigment vibrations and broad phonon wings due to low-frequency protein vibrations. The electron-phonon coupling is defined by the density of states of the protein phonons and the Huang-Rhys factor S which represents the coupling strength. It characterizes the average number of phonons following a certain electronic transition [6].

The electron-phonon coupling will be described in Section 2.1.2 of this thesis.

1.3. Literature data

In order to better understand the spectroscopic properties of LHC II, Rogl et al. (2002) applied a site-directed mutagenesis and obtained four different forms of LHC II, each of them lacking a specific chlorophyll binding site. These mutant forms of LHC II have been refolded from overexpressed purified apoproteins, pigments, and lipids. Then, in the temperature range of 4—300 K the absorption spectra of obtained mutants were measured and compared to refolded intact LHC II complexes. Spectra acquired from the experiments allowed to assign spectral bands to the specific Chl molecules in the structure of LHC II (Figure 5) [13].

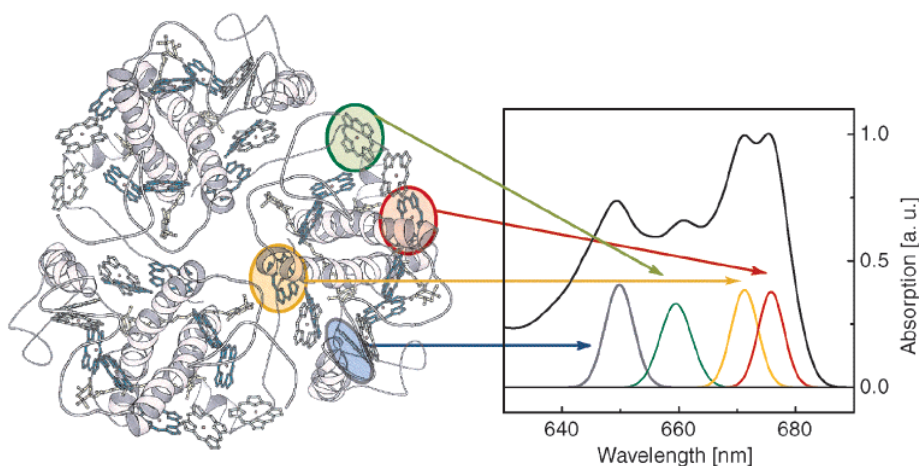


Figure 5: Assignment of spectral chlorophyll forms to related binding sites of the LHC II (view from the stromal side): blue — Chl b6; green — Chl b3; yellow — Chl a5; red — Chl a2 [13]. *Permission obtained.*

Assigning chlorophyll molecules to the absorption of specific wavelengths helps to understand the absorption spectrum of LHC II. The 3D map of LHC II constituents and their related spectral features in Figure 5 above is essential for the description of the excitation energy transfer (EET) in the LHC II complex.

Modelling the excitation energy transfer (EET) in LHC II is a key part to understand LHC II. Excitation dynamics have been modelled at a quantitative level with the use of time-resolved spectroscopic techniques. Such modelling experiments helped to find structural assignment of certain rates to specific energy transfer pathways from certain chlorophylls to others. The energy level diagram together with relaxation time constants for the LHC II monomer have been modelled by van Grondelle and Novoderezhkin in 2005 (Figure 6) [14].

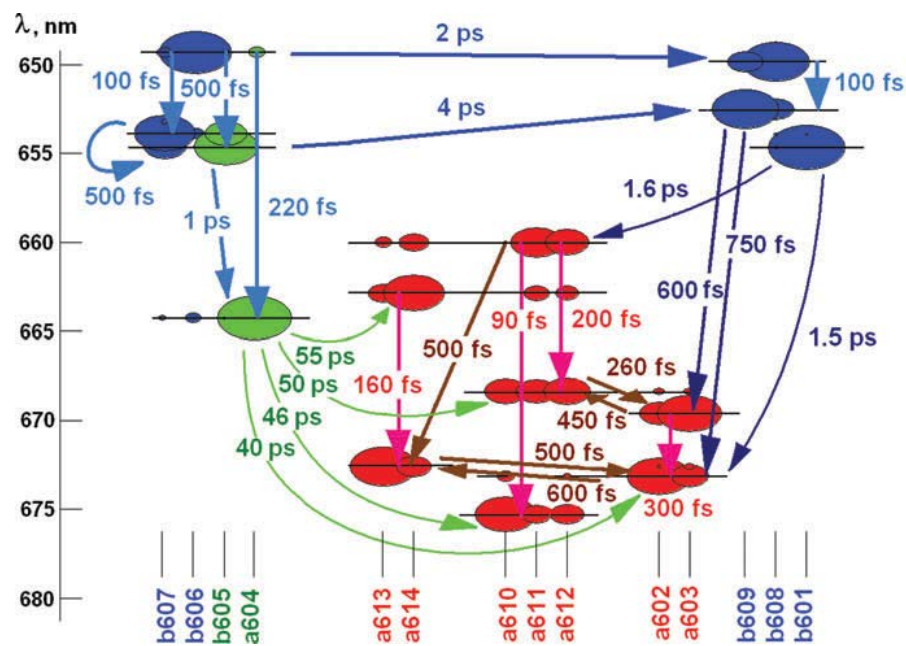


Figure 6: Energy-level diagram of the LHC II monomer. The wavelengths (positions) of the 14 exciton levels, pigments corresponding to these exciton levels and their relaxation time constants are given [14]. *Permission obtained.*

The Chl *a* region in Figure 6 above is determined by the three-level *a610-a611-a612* trimer, and the two-level *a602-a603* and *a613-a613* dimers. Intra-cluster relaxation (red arrows) in the Chl *a* region occurs in 90-300 femtoseconds (fs), while inter-cluster energy transfers (brown arrows) take place in the 250-600 femtoseconds range.

The Chl *b* region comprises of the *b601-b608-b609* cluster with intra-relaxation times of 100 fs and a following energy transfer to Chl *a* clusters at sub-picoseconds (ps) rate. Another cluster of *b607-b606-b605-a604* has an intra-cluster energy transfer rate of 100 fs-1 ps, while later energy transfers from *a604* to other Chl *a* clusters happens at slower rates — 40-55 ps.

The model described above allows to determine timescales and pathways of excitation energy transfers in the LHC II complex, which leads to the picture of pigment-protein interactions in order to store solar energy.

The purpose of this thesis is to analyze the effects of pigment-pigment interactions and protein dynamics at low and elevated temperatures by combining optical spectroscopy and quasielastic neutron scattering methods. In particular:

- to analyze the temperature-dependent absorption data of LHC II mutants lacking certain pigment molecules;
- to analyze temperature-dependence of the protein dynamics of LHC II investigated by quasielastic neutron scattering (QENS); and
- to reveal or gather information on the excitonic low-energy level structure of LHC II and its temperature dependence.

This thesis presents the results of the data analysis of the experiments involving intact LHC II and LHC II mutants.

2. Materials and methods

2.1. Lineshape of absorption bands

When analysing conventional absorption and flu spectra of trimeric LHC II, it results in broad absorption and fluorescence spectra without structure. In pigment-protein complexes, there is a large inhomogeneous broadening ($\sim 100\text{--}300\text{ cm}^{-1}$) that hides most information about energy levels and electron-phonon coupling [6]. Different line-narrowing methods, such as spectral hole-burning and difference fluorescence line-narrowing can be used complementarily for obtaining information on homogeneously broadened spectra.

2.1.1. Homogeneous and inhomogeneous broadening

According to the McGraw Hill Science & Technology Dictionary, inhomogeneous broadening is defined as “an increase beyond the natural linewidth in the width of an absorption or emission line that results from a disturbance that can differ from one source emitter to another.” [15]

As mentioned in Section 1.2, the transition frequency of the pigment-protein molecules is affected by the specific protein environment. If pigments would be enclosed into a perfect crystal, the environment would be similar for equivalent binding site molecules. Therefore, for all pigment molecules the optical transition would be at the same frequency. In other words, absorption and fluorescence spectra of those pigments would be homogeneously broadened. But since the pigments are embedded into protein matrices, the local environment of individual pigments at identical binding sites differs significantly in proteins. Because of that, the resulting absorption and fluorescence spectra will be inhomogeneously broadened [6].

Inhomogeneously broadened spectra can be expressed with the following equation:

$$L(\omega) = \sum_{R=0}^{\infty} \left(S^R \frac{e^{-S}}{R!} \right) \int d\Omega_0 N(\Omega_0 - \omega_c) l_R(\omega - \Omega_0 \mp R\omega_m). \quad (2)$$

where:

- $R\omega_m$ — absorption
- + $R\omega_m$ — fluorescence
- $N(\Omega_0 - \omega_c)$ — Gaussian inhomogeneous distribution function
- $l_R(\omega - \Omega_0 \pm R\omega_m)$ — one phonon profile
- S — Huang-Rhys factor
- R — total number of phonon transitions

In order to remove inhomogeneous broadening from the pigment-protein complex, spectral line-narrowing spectroscopy methods can be used.

2.1.2. Electron-phonon coupling

Since LHC II consists of arrays of pigment molecules that are located very close to each other, excitonic interactions have to be taken into account (as described at the end of the previous section). The exciton is a bound state of a hole and an electron. Being an elementary excitation of the condensed matter, it is able to transfer energy without transferring net electric charge. For photosynthesis, Frenkel excitons are the relevant excitons. In Frenkel excitons, the electron and hole propagate together and reside in one molecule. Various approaches — such as time-resolved spectroscopy, single molecule spectroscopy and two-dimensional electronic spectroscopy — were used to study pigment-pigment and pigment-protein interactions, the excitonic energy level structure and the dynamics of the photosynthetic antenna complexes [16].

Besides that, photosynthetic antenna complexes exhibit electron-vibrational coupling. The electron-vibrational coupling is an interaction between the molecular transition of electrons and the intramolecular nuclear vibrations. Together they define the vibronic structure of an individual pigments' (chromophores) optical spectra. Chromophore-host interaction — which is a case of electron-vibrational coupling in photosynthetic complexes — leads to the electron-phonon structure of the spectra. Phonons are protein vibrations at low frequencies in pigment-protein complexes [16].

The electron-phonon coupling occurring in pigment-protein systems is schematically explained in Figure 7 below. Two parabolic wells in Figure 7 show the potential of the protein vibrations in the ground and excited states. The shift of their equilibrium position is labeled with a_k . Intense and weak transitions between the vibrational levels are shown by thick and thin arrows respectively. After excitation at low temperature and subsequent thermal equilibrium, only the lowest phonon level of the excited state is occupied. That means that there are no excited phonons. The wavefunction of the lowest phonon level of the excited state overlaps with the lowest phonon level of the ground state, which makes the electronic transition without creating phonons possible. If such an electronic transition occurs without change in the phonon levels population it is called *zero-phonon transition*. Zero-phonon transitions form zero-phonon lines (ZPL) in spectra (right picture in Figure 7). Other transitions can create certain numbers of phonons, and are respectively referred to as one-, two-, three-, n-phonon transitions. Spectral changes related to the change in the population

of phonon levels are viewed as the phonon sideband (PSB). As it has been mentioned earlier, the average number of phonons associated with a particular electronic transition is measured by Huang-Rhys factor S . [6].

The energy released during the process of equilibration of the phonon levels is called reorganization energy. Electron-phonon coupling induces a mirror symmetry between absorption and fluorescence spectra called the Stokes shift. The energy difference of the Stokes shift equals two times the reorganization energy [16].

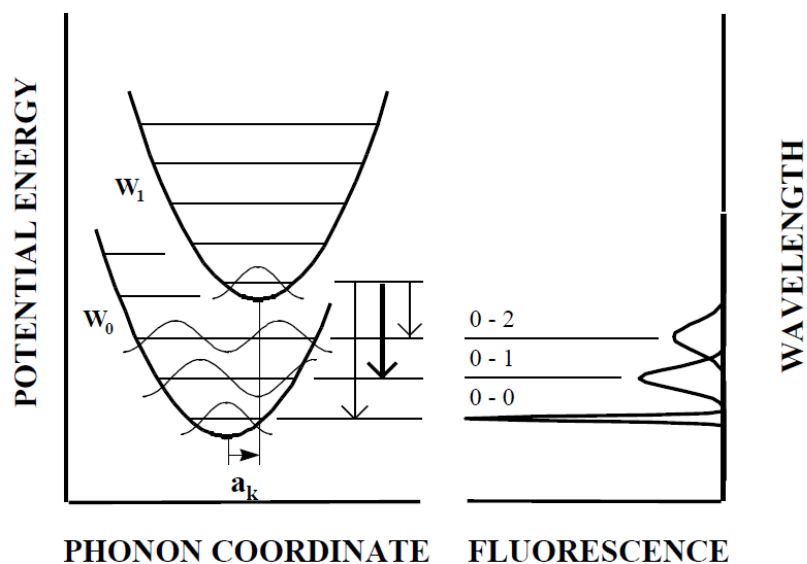


Figure 7: Left picture: Diagram of the potential energy of a pigment coupled to protein vibrations (phonons). W_0 — parabolic potential of the protein vibrations in the ground state. W_1 — parabolic potential of the protein vibrations in the excited electronic state. a_k — the shift of their equilibrium position. Thick arrows — intense transitions between the vibrational levels. Thin arrows — weak transitions between the vibrational levels.

Right picture: Relevant zero-phonon (0-0), one-phonon (0-1) and two-phonon (0-2) transitions of the fluorescence spectrum [6]. *Permission obtained.*

Electron-phonon and electron-vibrational interactions form homogeneously broadened spectra of the photosynthetic pigment molecules. In spectra measured by conventional absorption or fluorescence spectroscopy this structure is hidden by the inhomogeneous broadening (see Section 2.1.1) caused by the heterogeneity of the protein environment. To unravel the homogeneously broadened spectra from the inhomogeneous broadening, line-narrowing spectroscopy has shown to be effective.

2.2. Quasielastic neutron scattering (QENS)

Quasielastic neutron scattering is applied to study protein dynamics, which is very important to understand the functioning of proteins [17].

First, we will take a look on the definition of a neutron, the working principles of neutron scattering, and then review the quasielastic neutron scattering method in the study of protein motions in PS II membrane fragments containing the antenna complex LHC II.

Neutrons are particle waves. Their energy E and wavelength λ are related by the following formula:

$$E = \frac{2\pi^2\hbar^2}{m} \frac{1}{\lambda^2} E = \frac{2\pi^2\hbar^2}{m} \frac{1}{\lambda^2} \quad (3)$$

where: $\hbar = h/\pi$;

h — Planck's constant;

$m = 1.67 \times 10^{-27}$ kg (neutron mass)

A nuclear reactor typically provides “cold” neutrons with energies and wavelengths in the following ranges, if equilibrated at a temperature of about 30 K by a moderator:

$$1 \text{ meV} < E < 20 \text{ meV} \quad (4)$$

$$10\text{\AA} > \lambda > 2\text{\AA} \quad (5)$$

According to equations (4) and (5), it can be seen that the energies of the neutrons are in the low-energy dynamical excitations range, and the de Broglie wavelengths are in the order of interatomic distances. Thus, the neutron scattering method can show information about both structural and dynamical features of the samples. A schematic picture of the neutron scattering experiment is given in Figure 8.

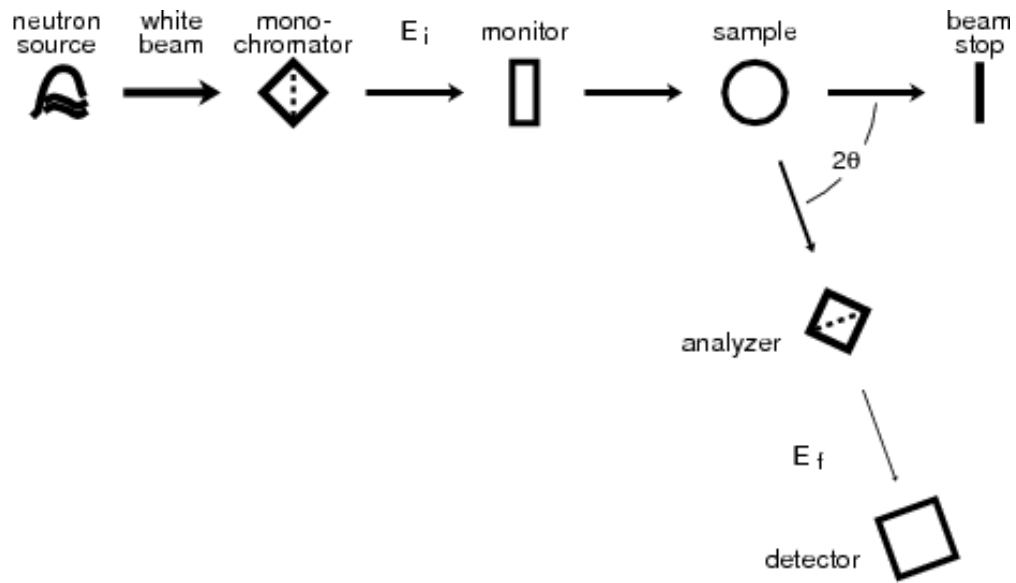


Figure 8: Scheme of the inelastic neutron scattering experiment [18].

When neutrons interact with a sample they exchange energy $\hbar\omega$ and momentum $\hbar\vec{Q}$ according to the following equations 6 and 7:

$$\hbar\omega = E_1 - E_0 \quad (6)$$

$$\hbar\vec{Q} = \hbar(\vec{k}_1 - \vec{k}_0) \quad (7)$$

where:

- \vec{k}_0 — wave vector of the incoming neutron
- \vec{k}_1 — wave vector of the scattered neutron
- E_0 — neutron energy of the incoming neutron
- E_1 — neutron energy of the scattered neutron

There are two different types of neutron scattering:

1. If $\hbar\omega=0$, then there is no energy transfer between the sample and the neutrons. This is called **elastic** neutron scattering.
2. If $\hbar\omega \neq 0$, then there is energy transferred between the sample and the neutrons. This is called **inelastic** (INS) or **quasielastic** (QENS) neutron scattering.

While elastic neutron scattering is applied to reveal the structure of the sample, INS and QENS techniques are used for studying vibrations and conformational molecular motions on the atomic level, respectively.

Inelastic neutron scattering is used to measure well distinguished vibrations. QENS is used to measure lower energy excitations like thermally activated protein (side chain) motions. QENS/INS spectra consist of three segments: 1) a central elastic peak; 2) a widely symmetric quasielastic broadening around the central elastic peak; 3) and inelastic contributions at the higher energy transfers [19].

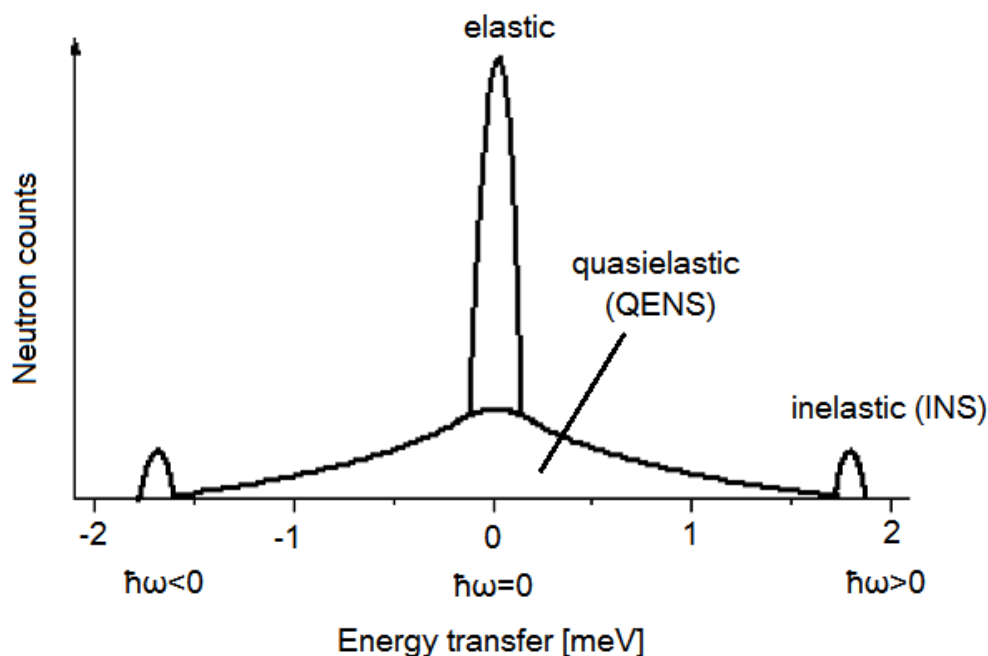


Figure 9: Composition of QENS spectra. The central elastic peak occurs when there is no energy transfer, i.e. $\hbar\omega=0$. There is a quasielastic broadening around the central elastic peak. Inelastic contributions are observed at $\hbar\omega<0$ and $\hbar\omega>0$.

In this study, we are focusing on quasielastic neutron scattering. QENS/INS experiments require a neutron source and well-adjusted spectrometers. A basic scheme of the process has been shown in a Figure 8 above. These types of experiments can be performed only in specialized research centers, of which there are only very few in the world. Examples are the Berlin Neutron Scattering Center, the Institut Laue Langevin in Grenoble, the Swiss Spallation Neutron Source, and a new facility, the European Spallation Source [20], which will be built in Lund, Sweden, from 2013 to 2020. Estonia is one of the partner countries in the European Spallation Source project.

QENS is used to obtain information about protein motions and internal molecular reorientations.

The dynamics of proteins largely depend on the environment. At low temperature, the LHC II system is in a crystalline state. This means that the system is trapped in different conformational substates. Dynamical transition corresponds to the onset of thermally activated motions of small protein side-groups between these substates. Their dynamical transition might be suppressed by dehydration, and affected by various solvents like sucrose or glycerol [21].

Despite the fact that a number of model protein have been studied using QENS, there are very few such studies for photosynthetic systems. These studies were conducted on PS II membrane fragments [22], the bacterial reaction center [23], the cyanobacterial antenna complex phycocyanin [24], and the LHC II antenna complex [25].

There are several reasons why photosynthetic systems have been studied so rarely:

- They are very complex
- Large amounts of samples are needed because of the low flux of the neutron sources
- Refined H-D exchange procedures should be carried out in order to suppress buffer and solvent scattering, because they also contain hydrogen atoms which might contribute to the scattering intensity

Nonetheless, QENS studies show important correlations between protein motions and function, and it is essential to do further research in this area.

Pieper et al. have investigated protein dynamics in the photosystem II (PS II) membrane fragments in terms of temperature [22] and hydration [26], which will be briefly described in the following.

The QENS spectra in Figure 10 represent the number of scattered neutrons plotted in terms of energy transferred between the primary neutrons and the sample. At 44% r.h. (relative hydration), the QENS spectrum mostly contains an elastic peak, whereas for 66% r.h. and 90% r.h. quasielastic contributions around the elastic peak are visible. These three relative hydration levels are presented in Figure 10. Hydrated membrane fragments were used in order to minimize scattering effects from the solvent containing hydrogen. Also D₂O was used instead of H₂O to suppress hydration water molecules that are left (the incoherent scattering cross section of D is lower than H for about a factor of 40).

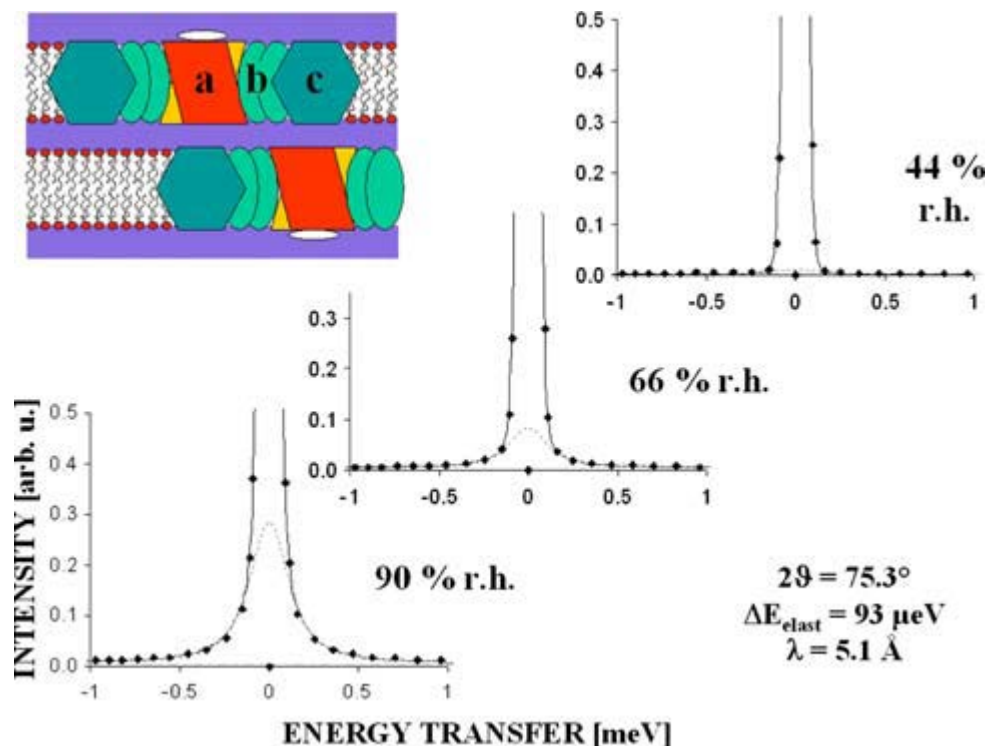


Figure 10: QENS spectra of the PS II membrane. Membrane fragments are hydrated in D₂O vapours with 44%, 66% and 90% r.h. Incident neutron wavelength: 5.1 Å; scattering angle: 75.3°; elastic resolution: 0.093 meV; temperature: 300 K. Black full lines are fits with one Lorentzian component (grey full lines). The elastic peak has been cut off at zero energy in order to investigate quasielastic points better. The coloured picture in the left upper corner shows a scheme of the hydrated PS II membrane system: a) reaction center; b) minor antenna complex; c) major antenna complex [26]. *Permission obtained.*

A similar approach has been used to investigate the dependence of protein dynamics on temperature by Pieper et al. in 2007 [22]. Hydrated and vacuum-dried membrane fragments of the photosystem II (PS II) taken from spinach (*Spinacia oleracia*) were investigated by QENS method in temperatures from 5 to 300 K. Three temperature regions are observed for protein dynamics. A) For temperatures below 120 K, protein dynamics for both hydrated and dry PS II fragments can be defined as harmonic vibrational motions. B) In the temperature range from 120 K to 240 K, protein motions are thermally activated. C) At temperatures above 240 K, protein motions are above the

“dynamical transition”. It has been seen that this dynamical transition depends on hydration, as for dry PS II membrane fragments it is strongly suppressed [22].

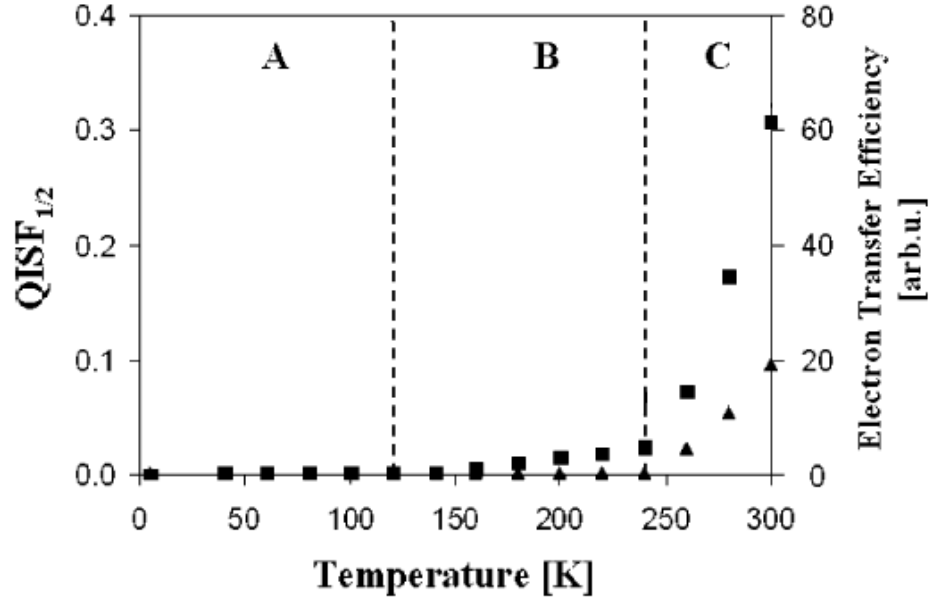


Figure 11: Temperature dependence of QISF1 (square points) and QISF2 (triangle points) for hydrated PS II membrane fragments. In region A, protein motions are “frozen”. In region B, protein motions are activated with the temperature increase. In region C, protein motions are above the “dynamical transition” [22]. *Permission obtained.*

Theoretical expression of the elastic (EISF) and quasielastic incoherent structure factors (QISF):

$$S_{\text{theo}}(\mathbf{Q}, \omega) = e^{-\langle u^2 \rangle Q^2} \left\{ A_0(\mathbf{Q}) \delta(\omega) + \sum_n A_n(\mathbf{Q}) L_n(H_n, \omega) \right\} \quad (8)$$

where:

Q — momentum of the neutron

ω — energy of the neutron

$\delta(\omega)$ — elastic component

$L_n(H_n, \omega)$ — a sum of quasielastic Lorentzian-shaped components

$A_0(Q)$ — elastic incoherent structure factors (EISF)

$A_n(Q)$ — quasielastic incoherent structure factors (QISF)

$e^{-\langle u^2 \rangle Q^2}$ — the Debye-Waller factor

The experimental scattering function is given in Equation 9:

$$S_{\text{exp}}(\mathbf{Q}, \omega) = F_{\text{N}} R(\mathbf{Q}, \omega) \times S_{\text{theo}}(\mathbf{Q}, \omega) \quad (9)$$

where: \mathbf{Q} — momentum of the neutron

ω — energy of the neutron

F_{N} — normalization factor

$R(\mathbf{Q}, \omega)$ — convolution of an experimentally obtained resolution function

$S_{\text{theo}}(\mathbf{Q}, \omega)$ — theoretical model function describing the dynamics of the sample system.

The QENS measurement parameters and the data treatment routine for the trimeric LHC II data analyzed in this thesis are given in the following section.

2.3. Sample preparation and measurements

2.3.1. Preparation of the LHC II mutants

A convenient way to produce LHC II mutants is in vitro refolding. LHC II is one of the few pigment-protein complexes reconstituted from its components. Absorption spectroscopy carried out in low temperature confirmed that refolded LHC II resembles spectral characteristics of the native LHC II complex very well [27]. In vitro refolding of intact LHC II and LHC II mutants has been done as described in Rogl and Kühlbrandt (1999) [28]. Native LHC II was purified from spinach (*Spinacia oleracea*). Apoproteins of LHC II were overexpressed in *Escherichia coli* (*E. coli*) as inclusion bodies. Reconstituted LHC II and LHC II mutants were obtained by washing the prepared *E. coli* with buffers containing lipid, detergent, and pigments. A mix of Chlorophylls (*a/b* ratio of 1.35) and carotenoids purified from spinach were used for the refolding of LHC II. Three LHC II mutants — Chl *a*610, Chl *a*612, and Chl *b*606 — have been obtained for this experiment. The analysis of the pigments was performed by high-performance liquid chromatography (HPLC). For low temperature measurements, a photometer equipped with a liquid-helium cooled cryostat was

used. The preparation of reconstituted LHC II and LHC II mutants was carried out by Laura Wilk in the laboratory of Professor Werner Kühlbrandt at the Max-Planck-Institute Frankfurt, Germany.

In this thesis, the term “intact LHC II” refers to a reconstituted LHC II containing all chlorophylls. Meanwhile, an “LHC II mutant” lacks a specific chlorophyll molecule: Chl *a*612 mutant lacks Chl *a*612, and so on.

Both, intact and mutant LHC II were used for optical experiments.

The term “native LHC II” means that this LHC II complex has been isolated from the spinach chloroplasts — no refolding took place. Native LHC II has been used for quasielastic neutron scattering experiments.

2.3.2. Optical measurements of the LHC II mutants

The optical experiments analyzed within this work were performed by Dr. Margus Rätsep and Prof. Jörg Pieper in the laboratory of Prof. Arvi Freiberg at the University of Tartu.

A 0.3 m spectrograph (Shamrock SR-303i) has been used for recording all spectra. The spectrograph has been combined with an electrically cooled CCD camera (DV420A-OE). Spectral gratings with 1800 and 600 grooves/mm helped to obtain an optical resolution of 0.1 or 0.4 nm respectively. A He-bath cryostat (Utreks, Ukraine) was used to control the sample temperature.

2.3.3. QENS measurements of native LHC II

Quasielastic neutron scattering experiments for the native trimeric LHC II sample data analysis in this thesis were carried out at the time-of-flight spectrometer NEAT [29] at the Berlin Neutron Scattering Center (BENSC), Hahn-Meitner Institute, Berlin, Germany. The incident neutron wavelength for the QENS measurements was 5.1 Å (3.2 meV), and the elastic energy resolution defined by vanadium standard runs was 0.117 meV. Data obtained from the QENS measurements were corrected for empty cell contribution, normalized, and converted to the energy transfer scale using the program package Fitmo 4 [30].

3. Experimental results

Absorption and fluorescence spectra were measured for the LHC II mutants along with quasielastic neutron scattering measurements. The results are given below.

3.1. Optical experimental data about the LHC II mutants

This section consists of three sub-sections: absorption and fluorescence spectra of all LHC II mutants were measured and compared to the intact LHC II at a temperature of 4.5 K (Section 3.1.1); the absorption differences (intact LHC II minus LHC II mutant) are calculated for all three LHC II mutants (Section 3.1.2); finally, maximum and full width at half maximum (FWHM) values of the absorption difference spectra of LHC II mutants are plotted in a graph and compared to each other (Section 3.1.3).

3.1.1. Absorption and fluorescence spectra of the LHC II mutants at 4.5 K

Absorption and fluorescence spectra of LHC II mutants Chl *a*610 and Chl *a*612 as well as the absorption spectrum of LHC II mutant Chl *b*606 were recorded at 4.5 K. The obtained spectra were compared to the spectra of refolded intact LHC II complexes containing all chlorophyll molecules. Respective figures are given further in this section.

Comparing the absorption spectra of mutant Chl *a*612 and the intact LHC II (Figure 12) shows that this mutant is lacking absorption at ~677 nm. Considering that this lack of absorption is in the Chl *a* region, Chl *a*612 can be assumed to be responsible for the absorption of light at ~677 nm. Further changes in the absorption spectrum, e.g. at ~651 nm and ~672 nm, are happening due to several reasons: imperfections in the refolding of the mutant, binding chlorophylls to the wrong sites during reconstitution, and excitonic interactions with other chlorophylls may be altered. Spectra were normalized according to pigment content determined independently by HPLC.

The fluorescence spectrum of the mutant Chl *a*612 has shifted towards the blue region of light, meaning Chl *a*612 was contributing to the fluorescence at around ~679 nm.

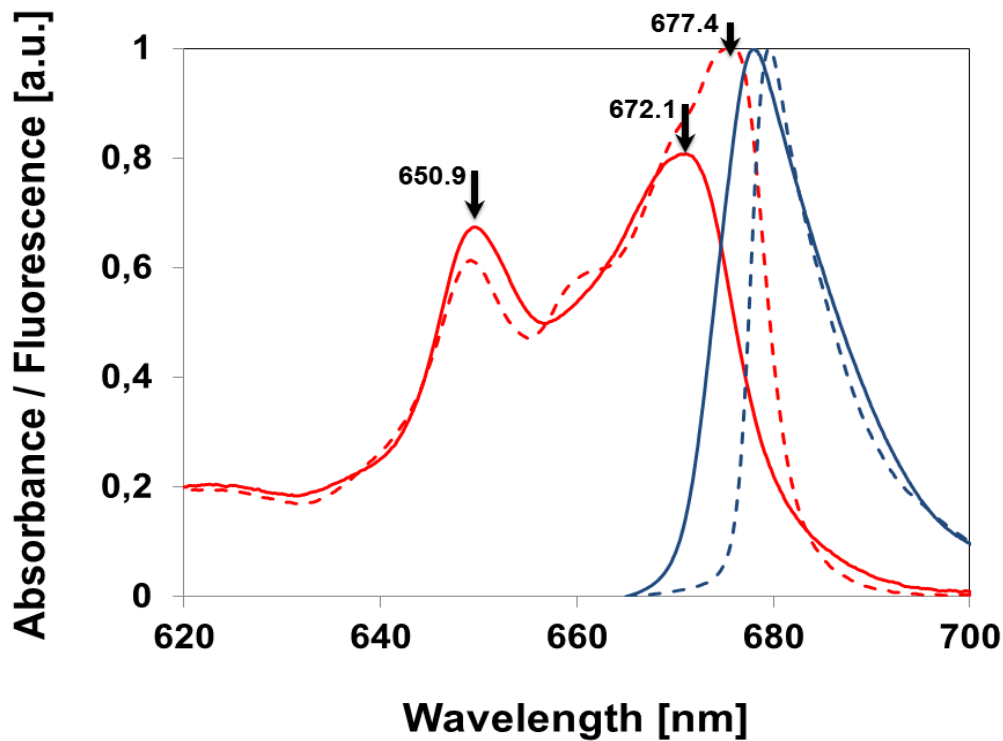


Figure 12: Absorption (full red line) and fluorescence (full blue line) spectra of LHC II mutant Chl *a612* compared to the absorption (dashed red line) and fluorescence (dashed blue line) spectra of the intact LHC II at 4.5 K.

The absorption spectra of the mutant Chl *a610* and of the intact LHC II are compared in Figure 13 below. Spectra were normalized according to pigment content determined independently by HPLC. From the figure it can be seen that the mutant Chl *a610* lacks absorption mainly at ~674 nm. Since it is a mutant lacking the Chl *a610* molecule, Chl *a610* appears to account for the light absorption at ~674 nm. Other small changes across the absorption spectrum can be caused by the fact that the mutant does not perfectly reflect native and refolded LHC II complexes. This can happen when chlorophylls are missing, as they are structural components. Since the mutant is a reconstituted complex, Chl *a* may be found in Chl *b* positions and vice versa. Also, chlorophylls are in close contact with each other, and may interact excitonically — meaning, if one of the interacting Chls is removed, the interaction will change.

In addition, the fluorescence spectrum of the mutant Chl *a610* has shifted towards the blue region of the electromagnetic spectrum of light which tells us that Chl *a610* was contributing to the fluorescence at ~679 nm.

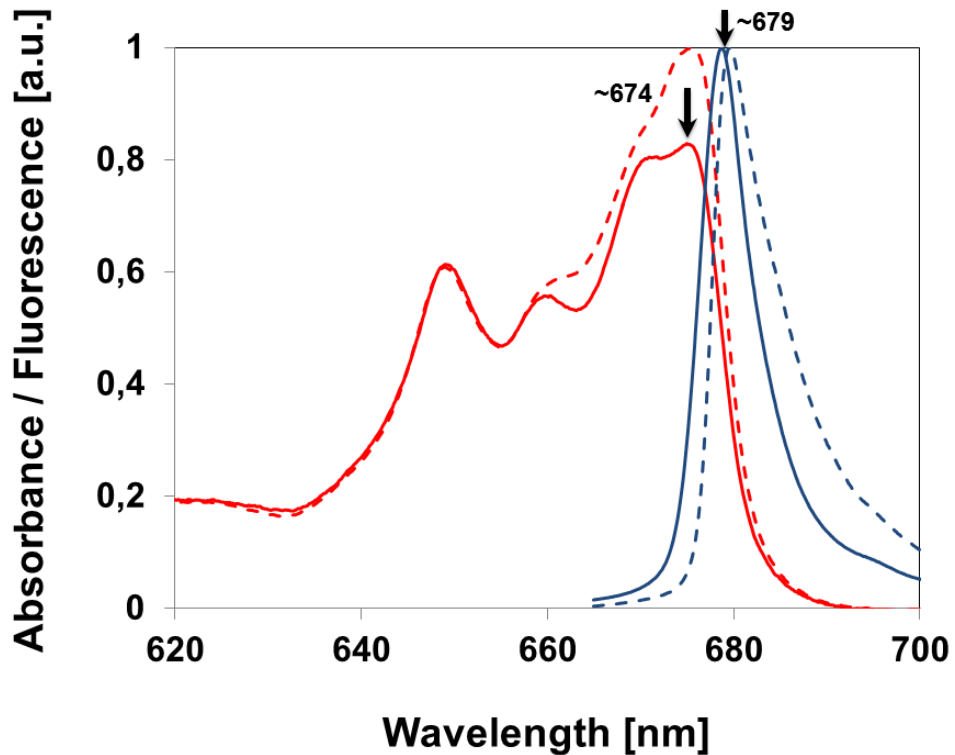


Figure 13: Absorption (full red line) and fluorescence (full blue line) spectra of LHC II mutant Chl *a610* compared to the absorption (dashed red line) and fluorescence (dashed blue line) spectra of the intact LHC II at 4.5 K.

Next, the absorption spectra of mutant Chl *b606* and the intact LHC II are compared (Figure 14). In this case, the Chl *b606* mutant is missing absorption primarily at around ~648 nm. This lack of absorption is in the Chl *b* region, which allows us to assume Chl *b606* to be responsible for the absorption at ~648 nm. Again, other small changes throughout the absorption spectrum of Chl *b606* mutant are occurring because of the reasons discussed above for Chl *a610* and Chl *a612* mutants: the mutant not resembling native and refolded LHC II complexes, Chl positions being exchanged and a change in the excitonic interactions of chlorophylls.

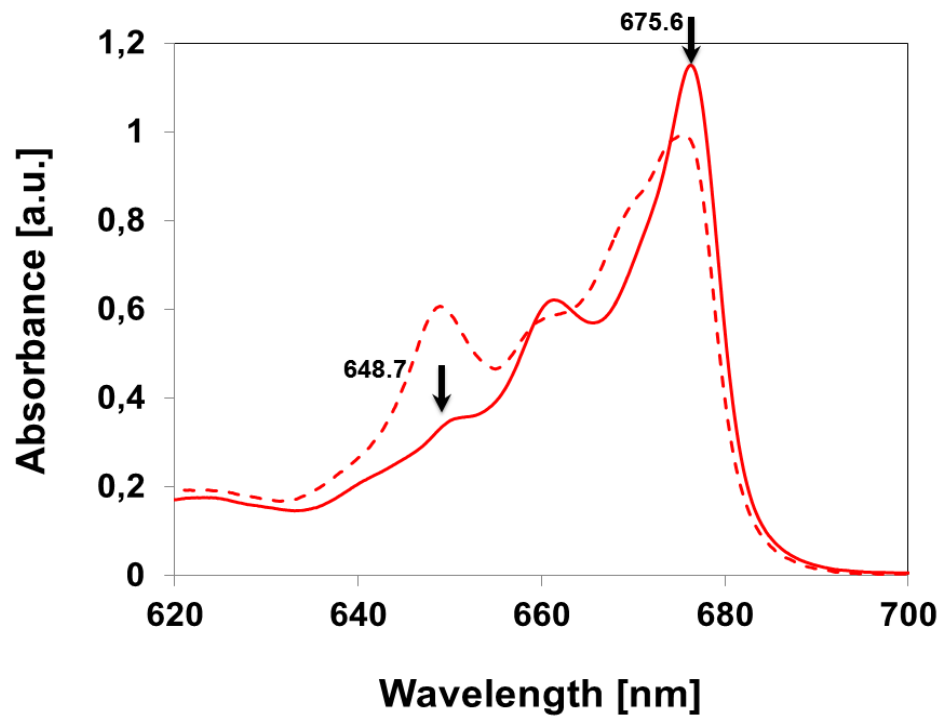


Figure 14: Absorption spectrum of LHC II mutant Chl b606 (full red line) compared to the absorption spectrum of the intact LHC II (dashed red line) at 4.5 K.

3.1.2. Absorption difference spectra of the LHC II mutants

Absorption spectra of LHC II mutants Chl *a612*, Chl *a610* and Chl *b606* have been measured for the temperature range from 4.5 K to 290 K. Then, absorption difference spectra — intact LHC II minus mutants — have been compiled. The resulting plots are given in this section.

Absorption difference spectra for the LHC II mutant Chl *a*612 are plotted in Figure 15. The peak positions of the absorption difference spectra are constant at lower temperatures, and then start constantly shifting towards longer wavelengths with increasing temperature. The height of the peak positions are decreasing with increasing temperature, while the spectra are broadening.

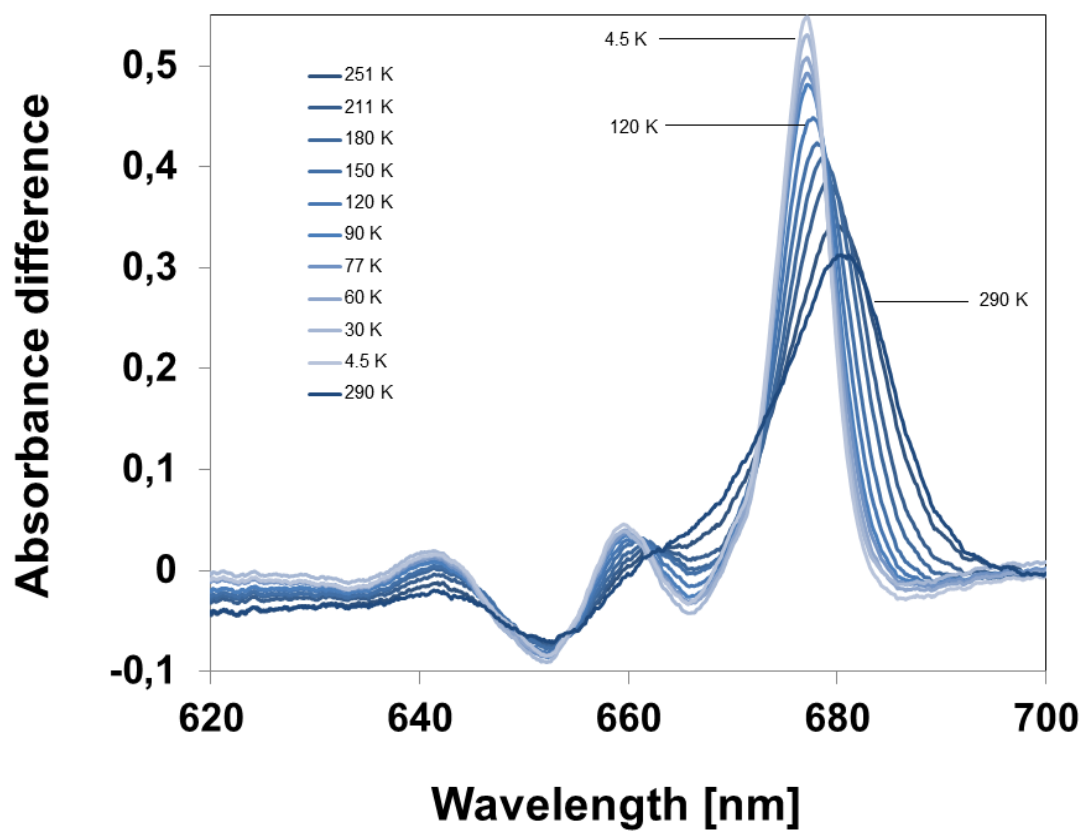


Figure 15: Absorption difference spectra (intact minus mutant) for LHC II mutant Chl *a*612. Spectra of the three temperatures — 4.5 K, 120 K, 290 K are indicated in the figure.

The absorption difference spectra for LHC II mutant Chl *a*610 are shown in Figure 16. From this figure it can be seen that with increasing temperature, absorption peak positions are first constant at the low temperature range, and then start slowly shifting to longer wavelengths. The height of the peak positions are decreasing and the spectra are broadening with higher temperatures.

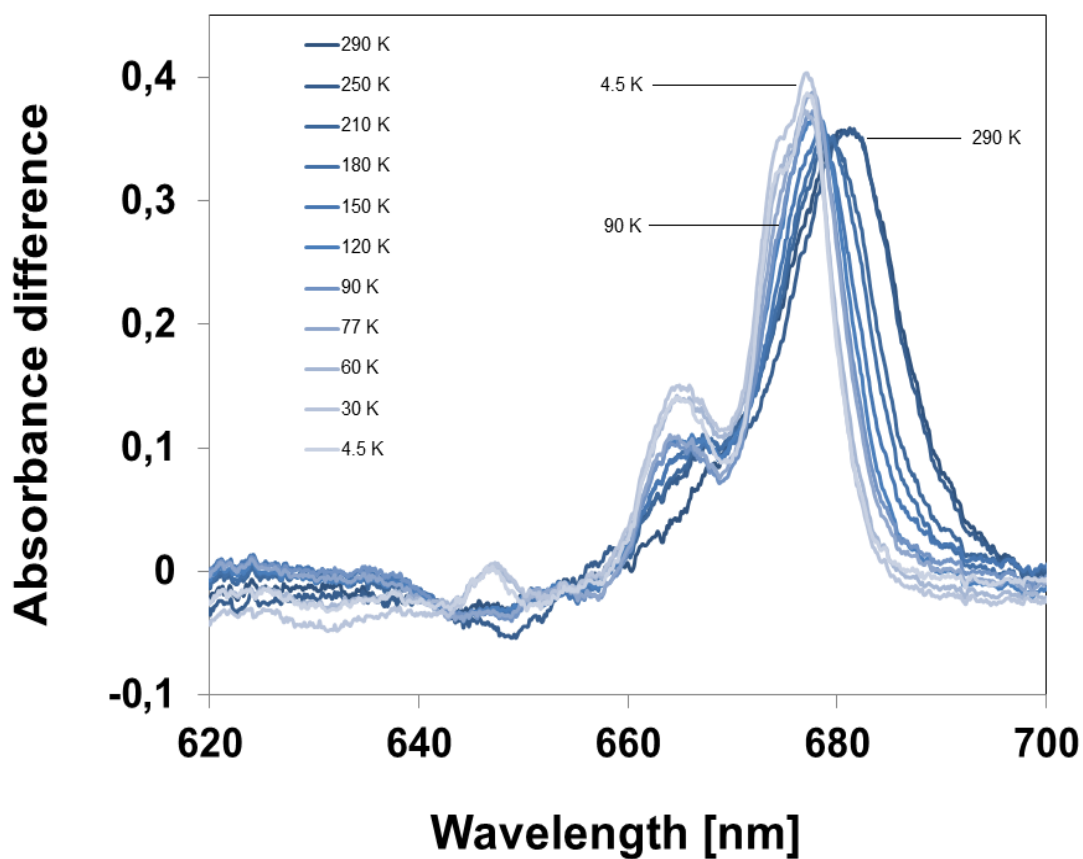


Figure 16: Absorption difference spectra (intact minus mutant) for LHC II mutant Chl *a*610. Spectra of the three temperatures — 4.5 K, 90 K, 290 K are indicated in the figure.

The absorption difference spectra for LHC II mutant Chl *b606* are given in Figure 17. For LHC II mutant Chl *b606* the positions of the absorption peaks are first stable at the lower temperature range and then start shifting to longer wavelengths with increasing temperature. At the same time, the spectra are getting broader at higher temperatures just as it has been observed for the other LHC II mutants.

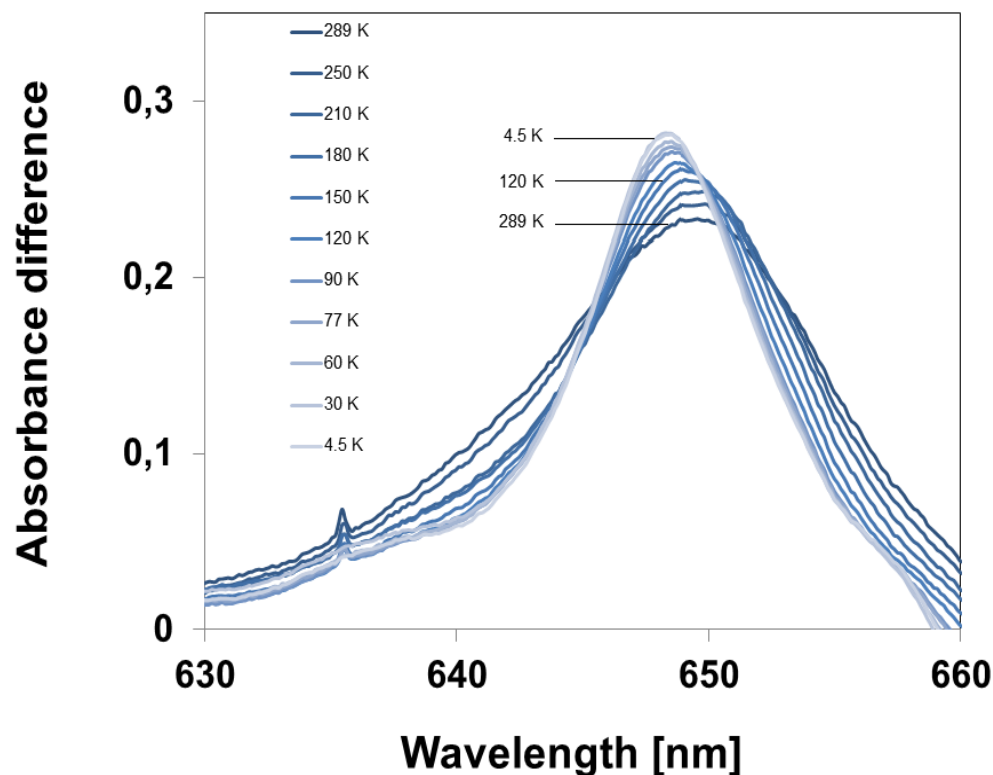


Figure 17: Absorption difference spectra (intact minus mutant) for LHC II mutant Chl *b606*. Spectra of three temperatures (4.5 K, 120 K, 289 K) are indicated in the figure.

3.1.3. Maximum and full width at half maximum (FWHM) values of the absorption difference spectra of the LHC II mutants

In this section, the peak positions of the absorption difference spectra of the LHC II mutants have been plotted as a function of temperature. In addition, temperature-dependent full width at half

maximum (FWHM) values of absorption difference spectra peaks have been added to the plots on secondary axes. Uncertainty ranges for both values are shown as black lines in the plots.

Peak positions and FWHM values of absorption difference spectra for LHC II mutant Chl *a*612 are shown in Figure 18. Peak positions are stable until 77 K, and then start shifting towards longer wavelengths. FWHM values are also increasing with increasing temperature.

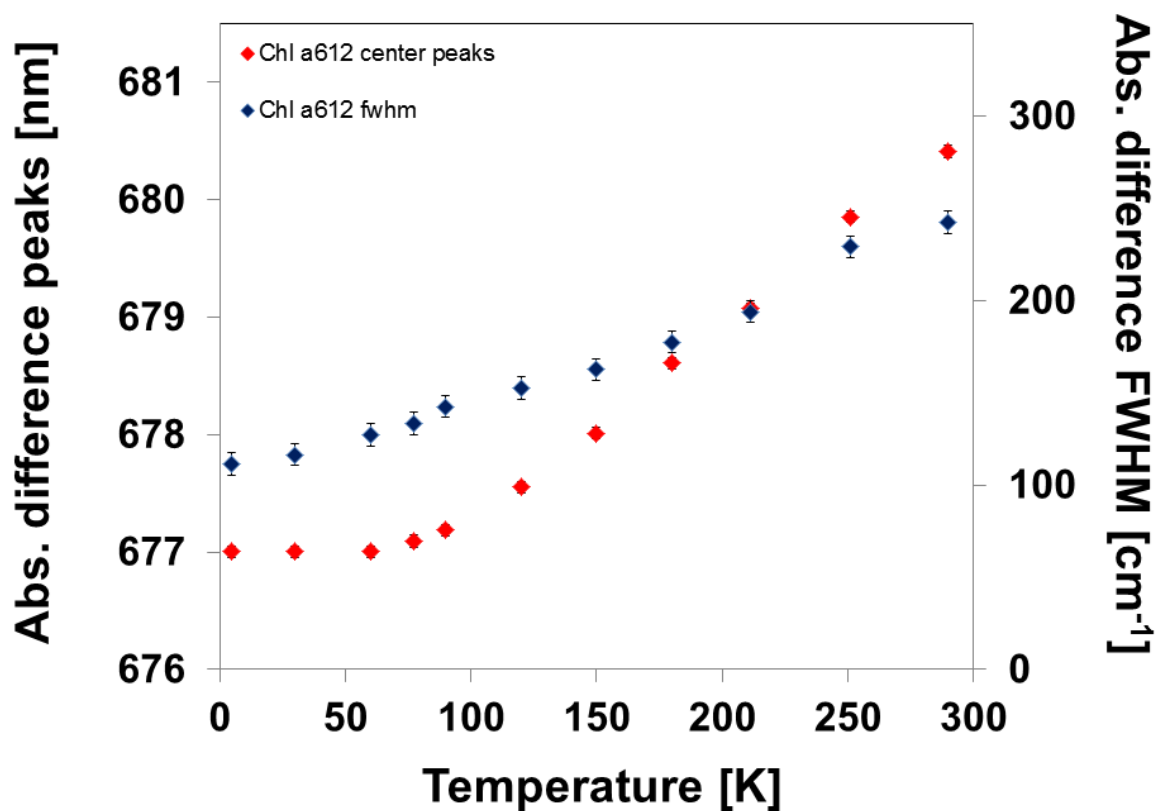


Figure 18: Temperature dependence of the maximum of LHC II mutant Chl *a*612 absorption difference band (red dots) compared to the temperature dependence of full width at half maximum (FWHM) values of LHC II mutant Chl *a*612 (blue dots). Uncertainty ranges are given.

For LHC II mutant Chl *a*610, peak positions and FWHM values of absorption difference spectra are given in Figure 19. In this figure it is more visible how the peak positions of the absorption difference spectra are first stable at lower temperatures, then start to shift to longer wavelengths with temperature increase over 77 K. Also, FWHM values are getting bigger with temperature increase in the same manner as the peak positions.

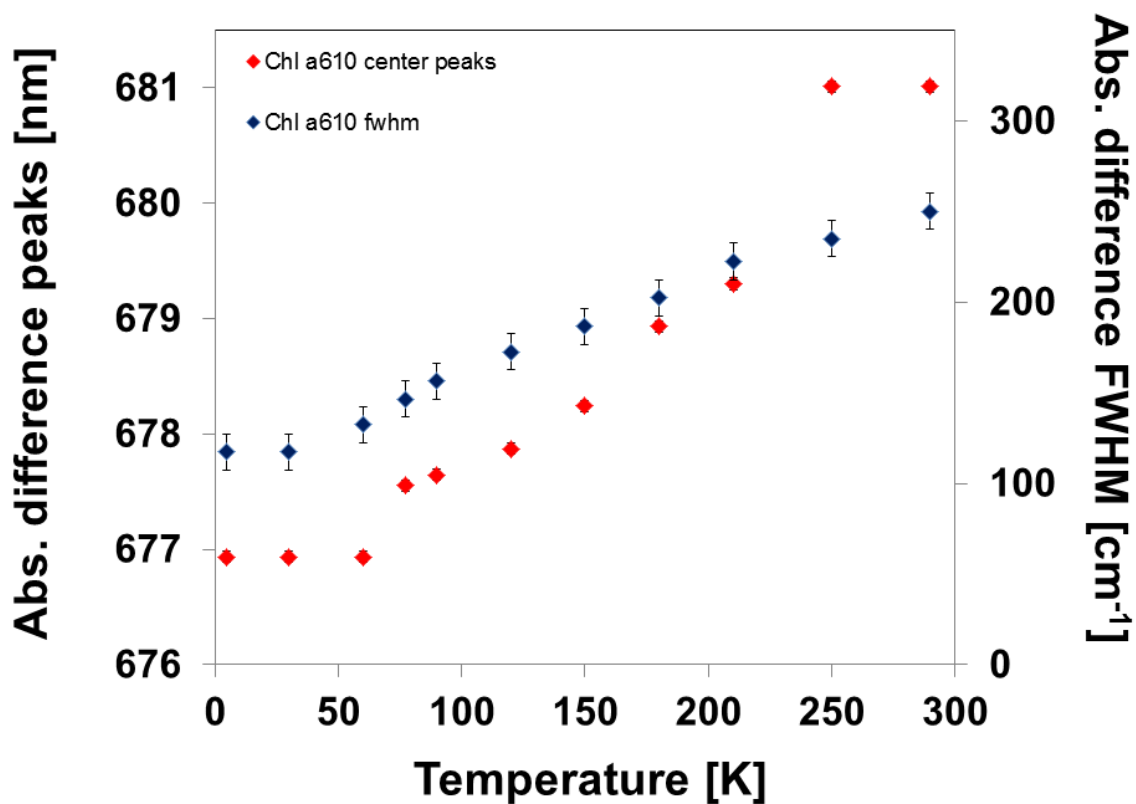


Figure 19: Temperature dependence of the maximum of LHC II mutant Chl *a*610 absorption difference band (red dots) compared to the temperature dependence of full width at half maximum (FWHM) values of LHC II mutant Chl *a*610 (blue dots). Uncertainty ranges are given.

Peak positions and FWHM values of the absorption difference spectra for LHC II mutant Chl *b606* are plotted in Figure 20 and basically act in the same way as for the other LHC II mutants. The peak positions of the absorption difference spectra of the Chl *b606* mutant are first stable until 77 K, and then start shifting towards longer wavelengths with the temperature getting higher. FWHM values of Chl *b606* are also stable at lower temperatures and get bigger with temperature increase.

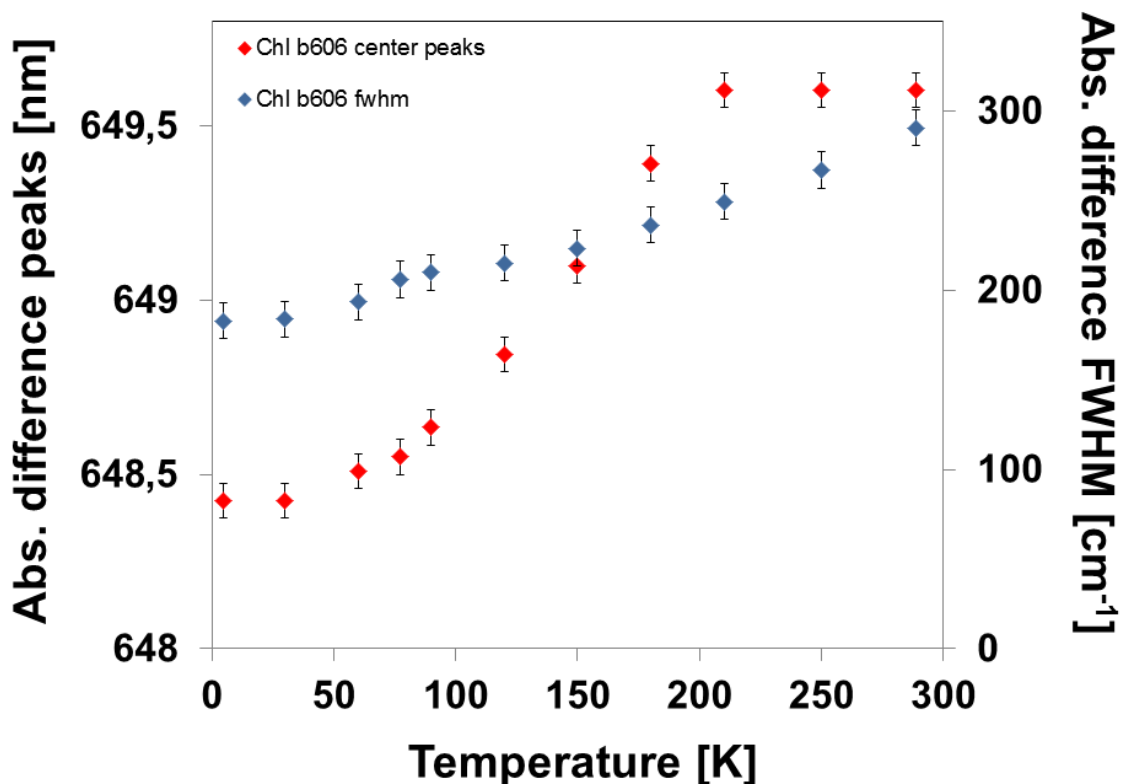


Figure 20: Temperature dependence of the maximum of LHC II mutant Chl *b606* absorption difference band (red dots) compared to the temperature dependence of full width at half maximum (FWHM) values of LHC II mutant Chl *b606* (blue dots). Uncertainty ranges are given.

3.2. Simulated fits of the LHC II mutants Chl *a612* and Chl *b606* absorption difference bands at 4.5 K

Fits for the LHC II mutants Chl *a612* and Chl *b606* absorption difference bands at 4.5 K according to Equation 2 are shown in Figures 21 and 22. As can be seen from the figures, the agreement of the fits with the experimental data is good.

The fits reveal the S-factors for Chl *a*612 and Chl *b*606 based on known one-phonon profiles for LHC II by Pieper et al. (1999) [31]. Others are free parameters obtained by fitting the absorption difference experimental data using the software Wolfram Mathematica [32].

In addition, a proper fit of the Chl *b*606 absorption band required a Voigtian profile to account for a significant Lorentzian lifetime broadening of 160 cm^{-1} .

Table 1 in the follow lists the parameters for the fit of Chl *a*612 and Chl *b*606 absorption difference band at 4.5 K in Figures 21 and 22 respectively.

Table 1

Parameters	Chl <i>a</i>612	Chl <i>b</i>606
ZPL peak	0	0
Inhomogeneous peak	0	0
Inhomogeneous width	110	70
Lorentzian width	—	160
Huang-Rhys factor 1	0.35	0.04
Phonon frequency 1	18	25
Gaussian phonon width 1	15	30
Lorentzian phonon width 1	90	90
Huang-Rhys factor 2	0.05	0.02
Phonon frequency 2	70	80
Gaussian phonon width 2	50	50
Lorentzian phonon width 2	200	200

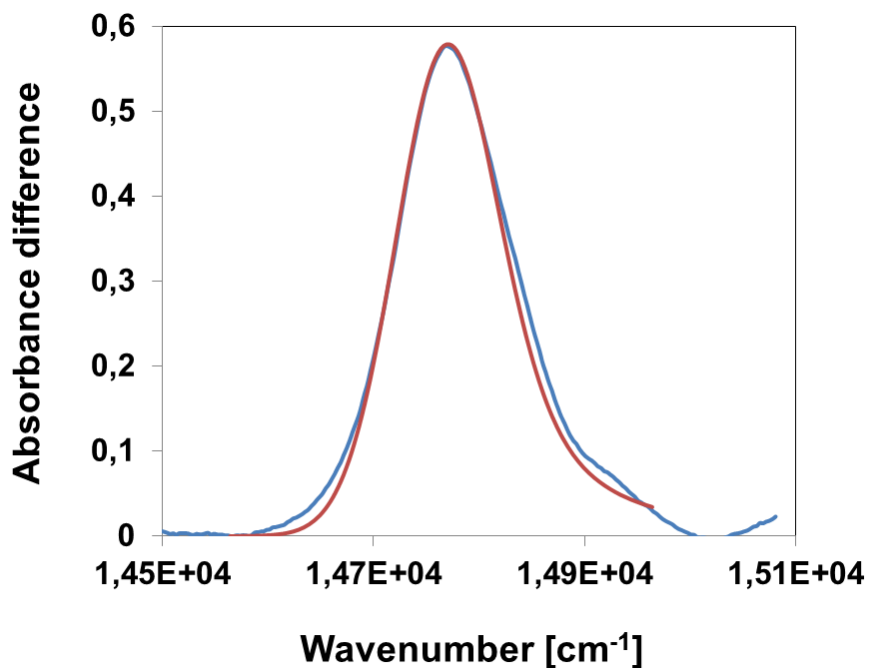


Figure 21: Simulated fit (dark red line) of the LHC II mutant Chl *a*612 absorption difference band (blue line) at 4.5 K.

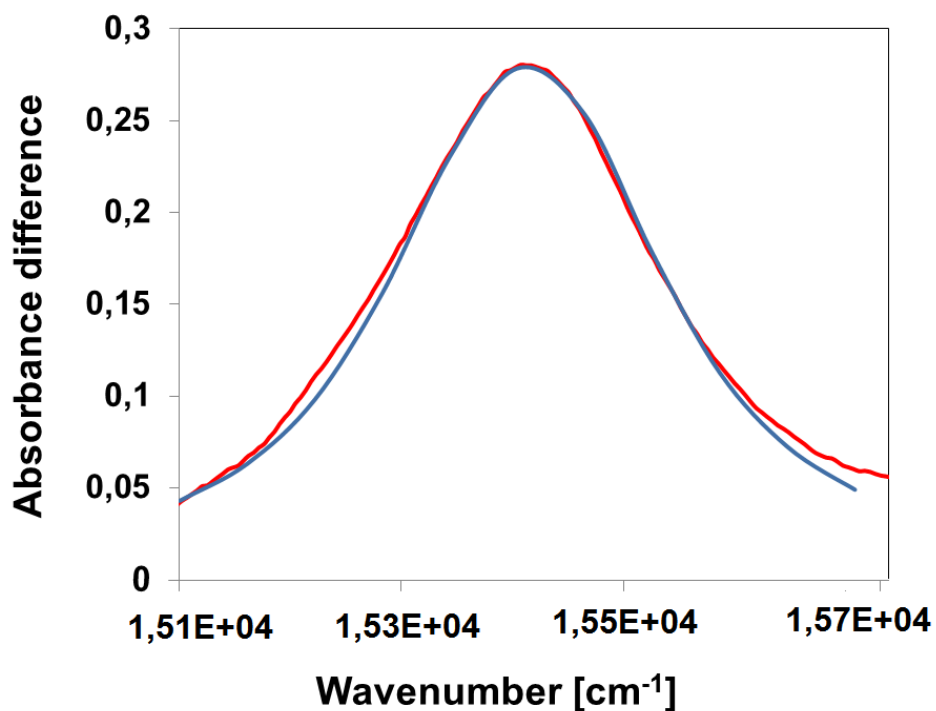


Figure 22: Simulated fit (dark red line) of the LHC II mutant Chl *b*606 absorption difference band (blue line) at 4.5 K.

3.3. Quasielastic neutron scattering experimental data about native LHC II

Data obtained from quasielastic neutron scattering experiments in the temperature range 20—305 K has been fitted with the program DAVE. The data obtained at 40 K was chosen as a resolution for the other data at higher temperatures, because it did not exhibit any quasielastic broadening. Then, the data was fitted using a quasielastic component with a Lorentzian width of 0.5073 meV and a flat background.

Data and fits for three temperatures are shown in Figure 23 below. From this figure it can be seen that the shape of the spectra resemble the QENS spectrum example given in Section 2.2. The spectra have an elastic peak at zero energy transfer, and quasielastic contributions around the peak.

The following tendencies are observed for our QENS spectra with increasing temperature:

- the Lorentzian contribution gets bigger,
- while the peak intensity of each data set gets lower.

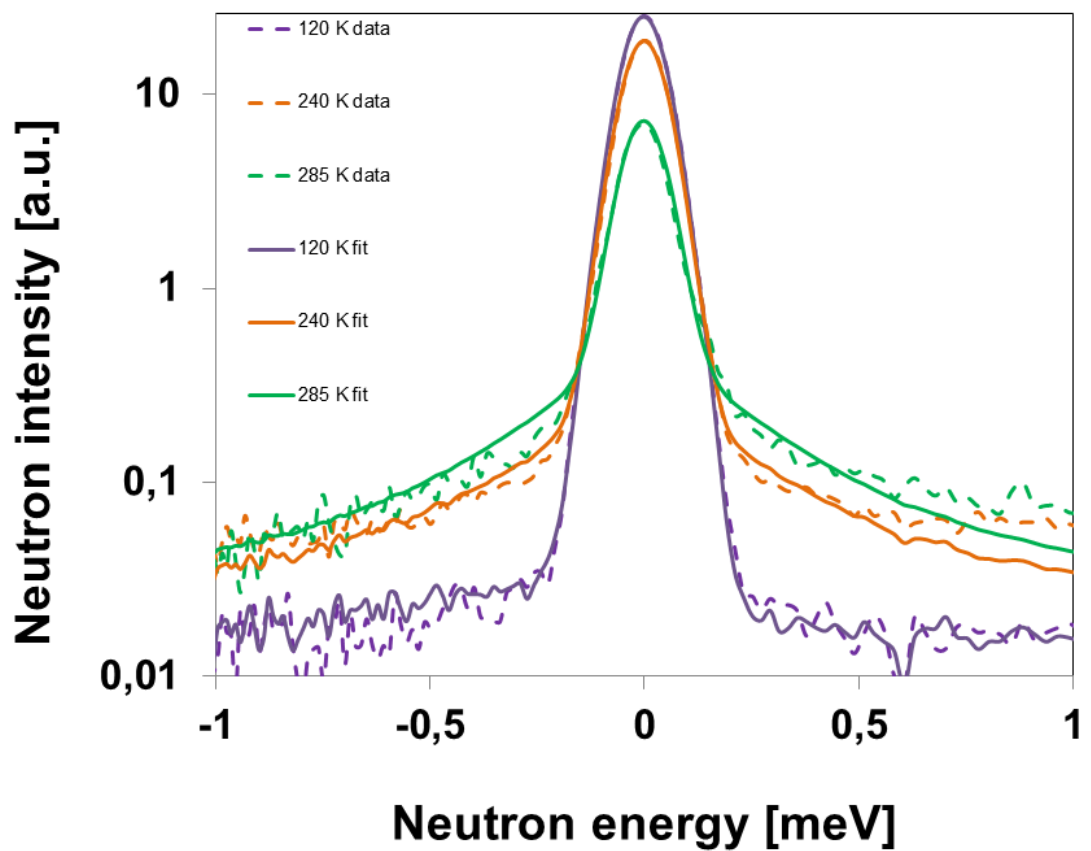


Figure 23: QENS data (dashed line) and fits (full line) and for three temperatures — 120 K, 240 K and 285 K. Note the logarithmic scale.

The relative Lorentzian intensities for all temperatures are referred to as quasielastic incoherent structure factor (QISF), while the relative elastic intensities are referred to as elastic incoherent structure factor (EISF). Then, by definition, the sum of QISF and EISF is one. QISF and EISF are plotted in Figure 24 and Figure 25 below.

The QISF plot is divided into three T-ranges:

- Range A — QISF points, i.e. protein motions in the native LHC II complex are “frozen”,
- Range B — protein motions are thermally activated,
- Range C — protein motion range that is above the “dynamical transition”.

If we recall Figure 11, described in Section 2.2 above, we can see a similarity with these two pictures.

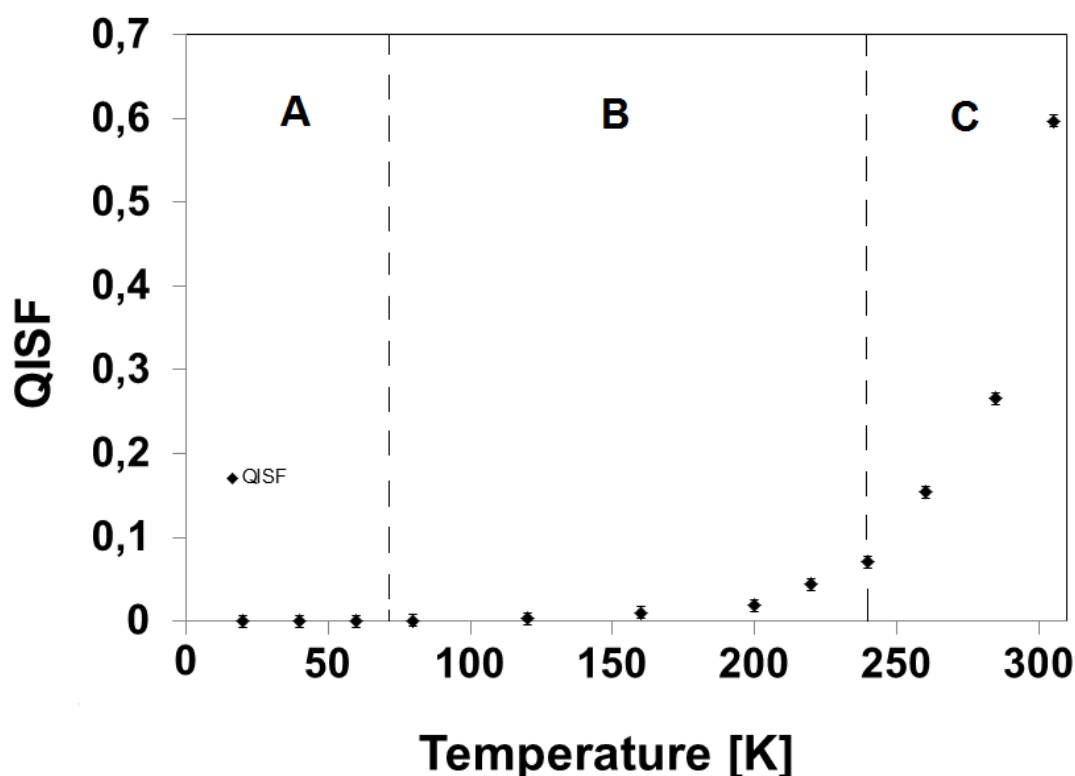


Figure 24: Temperature dependence of quasielastic incoherent structure factor (QISF) for native LHC II as obtained from the fits. In region A, protein motions are “frozen”. In region B, protein motions are activated with the temperature increase. In region C, protein motions are above the “dynamical transition”.

The EISF plot (Figure 25) has been compiled from the same data as the QISF plot above. The plot has been added to better see the protein motions and T-ranges. The EISF diagram is divided into three ranges: Range A with “frozen” conformational protein motions; Range B with thermally activated protein motions; and Range C with protein motions that are above the “dynamical transition”.

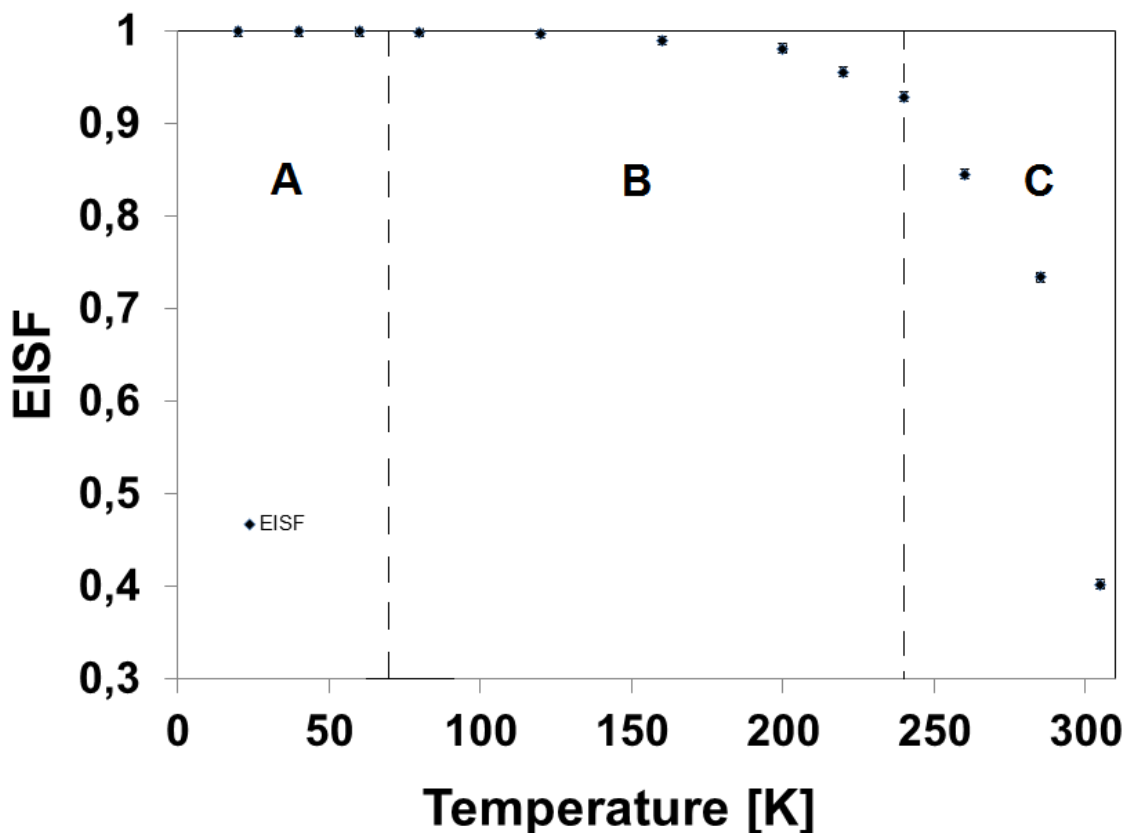


Figure 25: Temperature dependence of elastic incoherent structure factor (EISF) for native LHC II as obtained from the fits. In region A, protein motions are “frozen”. In region B, protein motions are activated with the temperature increase. In region C, protein motions are above the “dynamical transition”.

4. Discussion

4.1. Electron-phonon coupling in LHC II

4.1.1. Simulated fits of the LHC II mutants Chl *a*612 and Chl *b*606 absorption difference bands at 4.5 K

The Huang-Rhys factor S indicates the strength of the electron-phonon coupling. In this work, relatively low S -factors of 0.4 and 0.06 have been obtained from the simulated fits of the LHC II mutants Chl *a*612 (Figure 21) and Chl *b*606 (Figure 22) absorption difference bands at 4.5 K respectively. The fitting of the Chl *b*606 absorption difference band required the use of an additional Lorentzian contribution with a width of 160 cm^{-1} . Fitting the absorption difference spectra of the Chl *a*610 mutant has caused difficulties due to its three peak structure so that no fits are shown for this mutant. S -factors for the other temperature ranges have been obtained from the thermal broadening analysis according to Belgio et al. (2010) [33] and are given in the next section.

4.1.2. Linear fits of the FWHM values of the three LHC II mutants

The temperature dependence of FWHM values of the LHC II mutants Chl *a*610, Chl *a*612 and Chl *b*606 absorption difference spectra has been plotted in Figure 26 below. These FWHM values have been obtained in the T-ranges identified by QENS, i.e. in three temperature ranges: 4.5—60 K, 77—211 K, 240—290 K.

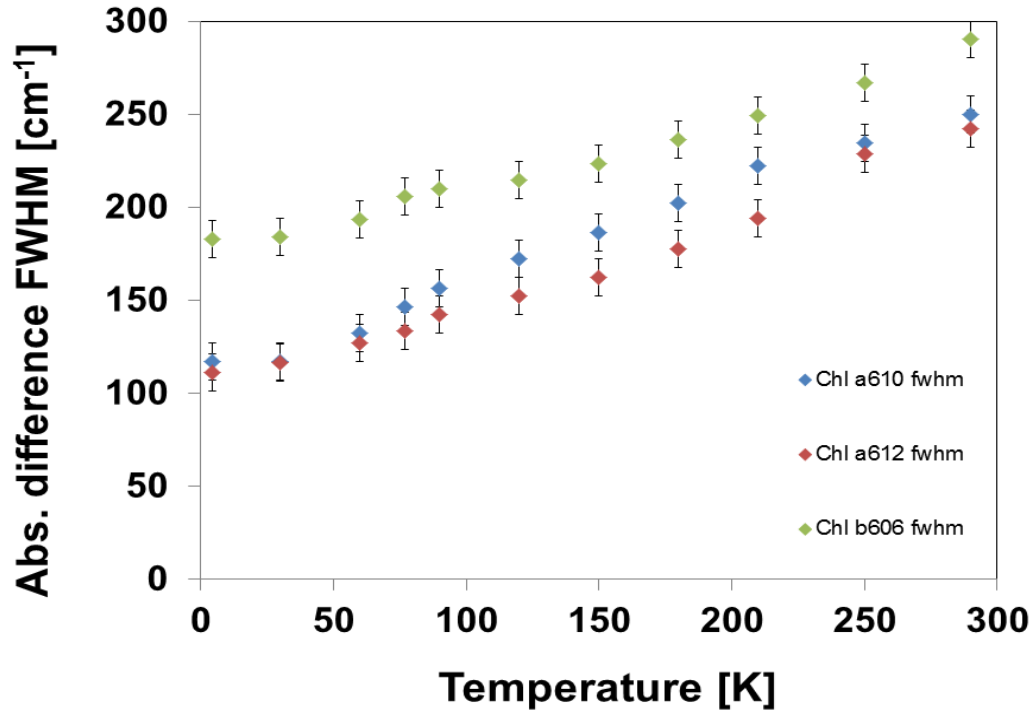


Figure 26: Temperature dependence of FWHM values of LHC II mutants Chl *a*610 (blue points), Chl *a*612 (red points) and Chl *b*606 (green points) absorption difference spectra. Uncertainty ranges are given.

In order to analyze these three temperature ranges of FWHM values of LHC II mutants three trendlines have been added to the square of the FWHM values for all mutants.

Square of the FWHM values plotted as a function of temperature for LHC II mutant Chl *a*612 is shown in Figure 27. Trendlines have been added for three temperature ranges: 4.5—60 K, 77—211 K and 211—290 K. The trendlines in Figure 27 show that slope is increasing discretely with the temperature: at 77 K and 211 K.

From the formula given in the thermal broadening analysis by Belgio et al. (2010) [33]:

$$\text{fwhm}^2 = 7.7Sv_mT + \text{fwhm}_{\text{inh}} \quad (10)$$

where: S — Huang-Rhys coupling strength

v_m (cm^{-1}) — mean phonon frequency associated with protein vibrations

T (K) — temperature

fwhm_{inh} — inhomogeneous broadening

we can calculate the S-factors for each temperature range of LHC II mutants. For example, by dividing the slope by 7.7 and the previously derived phonon frequency which equals 20, we can obtain the S-factors for each temperature range of the Chl *a*612 mutant:

For 4.5—60 K S-factor = $(67.15 / 7.7) / 20 = 0.44$
 For 77—211 K S-factor = $(140.37 / 7.7) / 20 = 0.91$
 For 211—290 K S-factor = $(268.41 / 7.7) / 20 = 1.74$

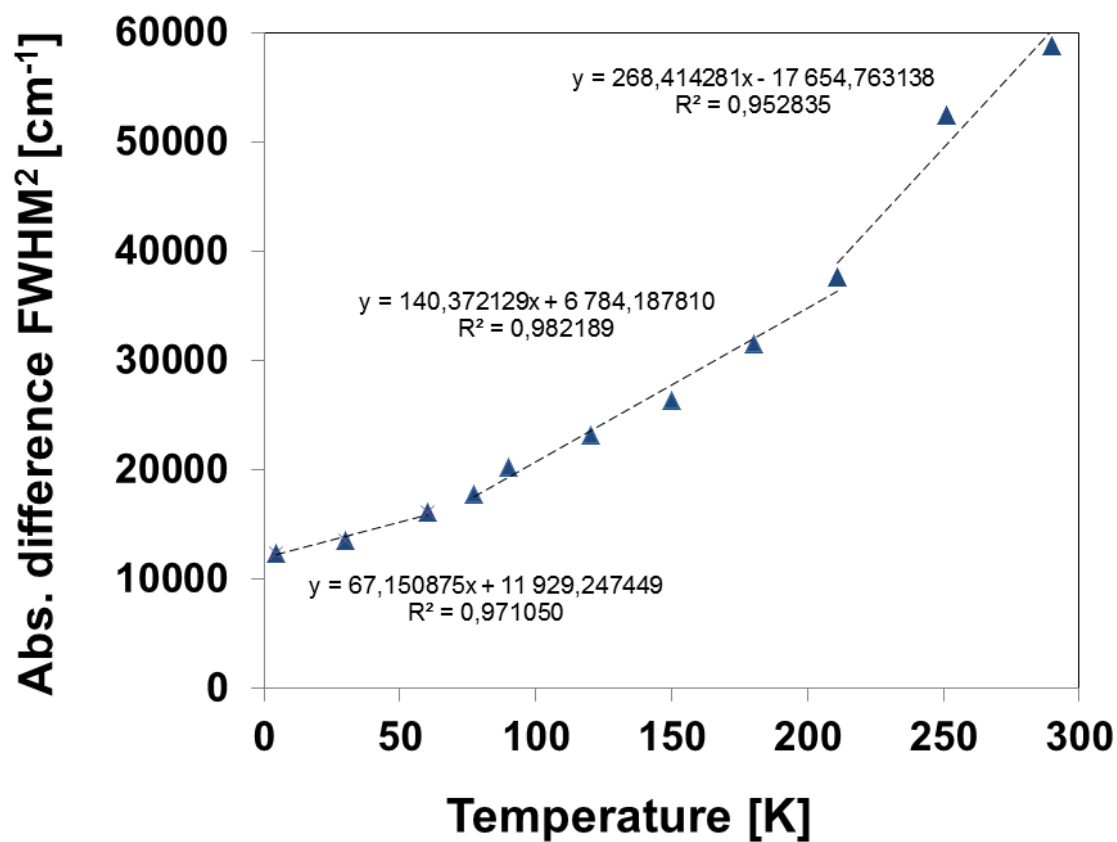


Figure 27: Square of the FWHM as a function of temperature for the absorption band of LHC II mutant Chl *a*612.

In Figure 28 square of the FWHM values for LHC II mutant Chl *a*610 have been plotted as a function of temperature. Same trendlines as for previous mutant have been added for three temperature ranges: 4.5—60 K, 77—211 K and 211—290 K. The slope of the trendlines of Chl *a*610 mutant is increasing with temperature. Just as for the previous mutant, by dividing the slope by 7.7 and the previously derived phonon frequency which equals 20, we can obtain the S-factors for each temperature range of the Chl *a*610 mutant:

- For 4.5—60 K S-factor = $(69.24 / 7.7) / 20 = 0.45$
- For 77—211 K S-factor = $(202.16 / 7.7) / 20 = 1.31$
- For 211—290 K S-factor = $(162.42 / 7.7) / 20 = 1.05$

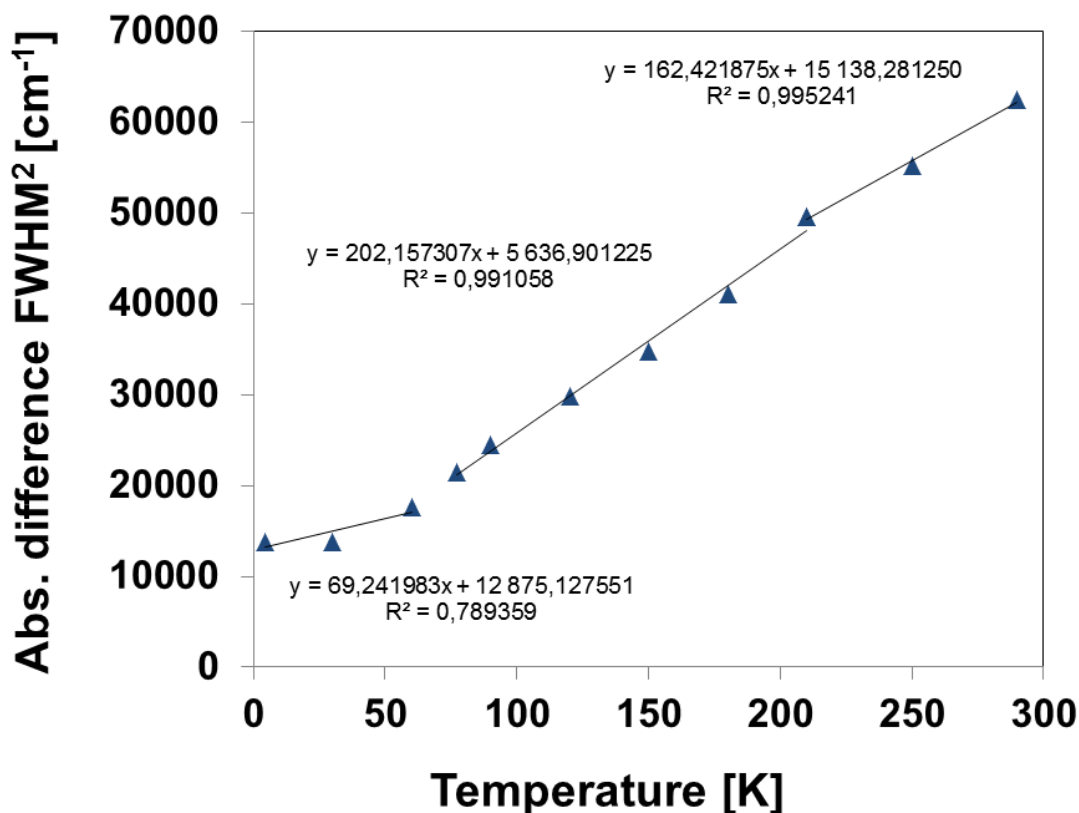


Figure 28: Square of the FWHM as a function of temperature for the absorption band of LHC II mutant Chl *a*610.

Square of the FWHM values for LHC II mutant Chl *b606* are given in Figure 29 as a function of temperature. Trendlines added into three temperature ranges show that their slope is increasing just as it has been observed for other two LHC II mutants before. For obtaining the S-factors for each temperature range, the slope is divided by 7.7 and the phonon frequency 20:

$$\text{For } 4.5\text{—}60 \text{ K} \quad \text{S-factor} = (72.64 / 7.7) / 20 = 0.47$$

$$\text{For } 77\text{—}211 \text{ K} \quad \text{S-factor} = (144.58 / 7.7) / 20 = 0.94$$

$$\text{For } 211\text{—}290 \text{ K} \quad \text{S-factor} = (280.02 / 7.7) / 20 = 1.82$$

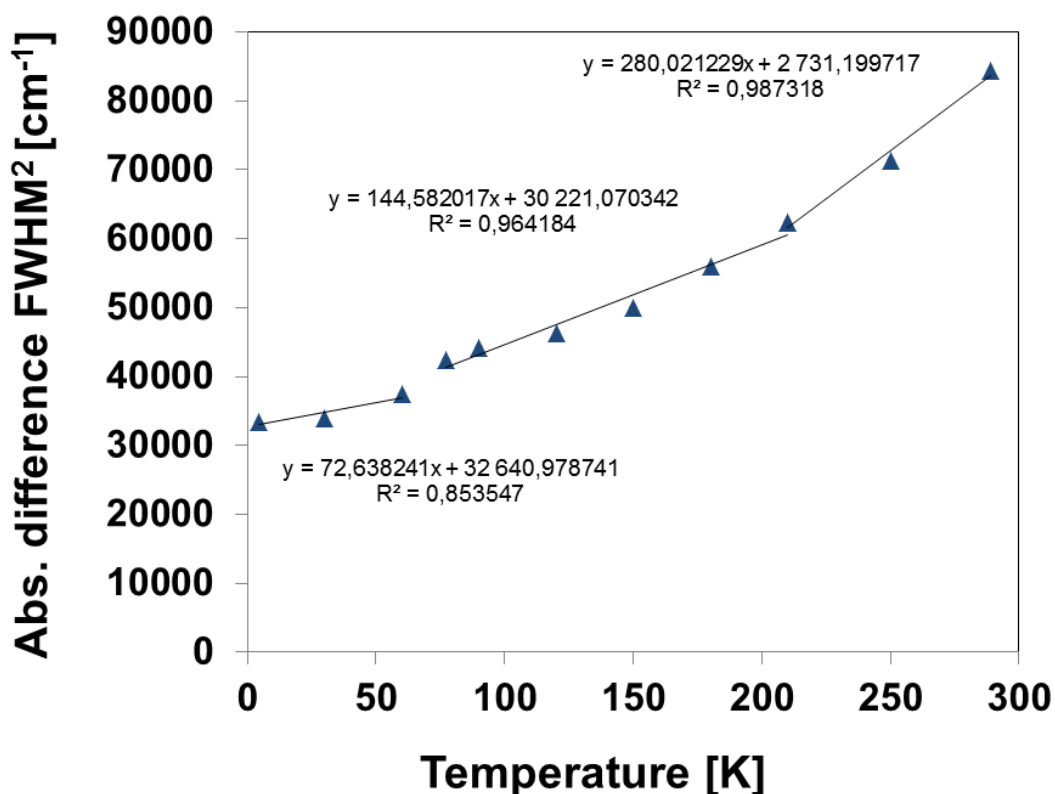


Figure 29: Square of the FWHM as a function of temperature for the absorption band of LHC II mutant Chl *b606*.

4.1.3. Table of the obtained S-factors for the LHC II mutants

The S-factors obtained from fitting the absorption difference peaks of Chl *a*612, Chl *b*606 and from the slope calculation of all three LHC II mutants have been collected in the Table 2 below.

Table 2

Mutants	Chl <i>a</i>610	Chl <i>a</i>612	Chl <i>b</i>606
From difference fits simulations	—	0.4	0.06
4,5—60 K	0.45	0.44	0.47
77—211 K	1.31	0.91	0.94
211—290 K	1.05	1.74	1.82

From this table it can be seen that the strength of the electron-phonon coupling is increasing with the temperature.

4.2. The role of the LHC II mutant Chl *a*612 for LHC II fluorescence at the temperature range from 4.5 K to 290 K

In the previous section it has been mentioned that Chl *a*612 is one of the contributors to the fluorescence of the LHC II complex at 4.5 K. In order to check if Chl *a*612 contributes to the fluorescence of LHC II at all temperatures, a comparison plot has been compiled, shown as Figure 30 below. From this figure it can be seen that at lower temperatures, from 4.5 K up to 150 K, Chl *a*612 is not the only contributor to the fluorescence of the native LHC II complex. However, starting from 150 K, the absorption difference peak positions of the Chl *a*612 mutant and the fluorescence peak positions of the native LHC II complex start shifting together. Above 150 K, the difference between those two lines in Figure 30 is 1 nm, just as in the Stokes shift ($2S\omega_m$). The calculation of the Stokes shift of the Chl *a*612 mutant for three temperature ranges is given below. The value of the

phonon frequency ν_m has been taken from independent spectral hole-burning analysis and equals 20 cm^{-1} .

$$\text{Stokes shift for Chl } a612 \text{ mutant (4.5—60 K)} = 2 * 0.44 * 20 = 17.6 \text{ cm}^{-1}$$

$$\text{Stokes shift for Chl } a612 \text{ mutant (77—211 K)} = 2 * 0.91 * 20 = 36.4 \text{ cm}^{-1}$$

$$\text{Stokes shift for Chl } a612 \text{ mutant (211—290 K)} = 2 * 1.74 * 20 = 69.6 \text{ cm}^{-1}$$

At 4.5—60 K, the measured Stokes shift (Figure 30) is $3 \text{ nm} = \sim 66 \text{ cm}^{-1}$, in our calculation it is 17.6 cm^{-1} , i.e. far too small. Therefore Chl *a612* is not the main contributor to the fluorescence. At the 77—211 K temperature range, the measured Stokes shift is $1 \text{ nm} = 22 \text{ cm}^{-1}$, in our calculation it is 36 cm^{-1} , but the $2S\omega_m$ equation overestimates the value, so this is a rather good agreement. Above 211 K, the calculated Stokes shift is larger than in Figure 30, which is qualitatively consistent. Fluorescence has different transition temperature, because thermal population of higher energy states causes a blue-shift, that has to be compensated by the red-shift due to protein dynamics. These facts lead us to the conclusion that Chl *a612* is a major contributor to the fluorescence of the LHC II complex at elevated temperatures.

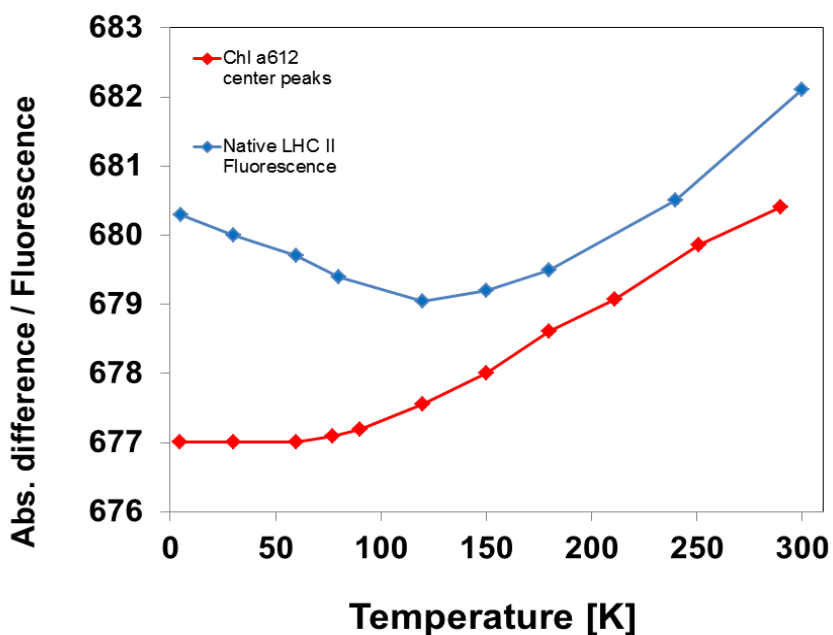


Figure 30: Temperature dependence of the maximum of LHC II mutant Chl *a612* absorption difference spectra (red dots connected with line) compared to the temperature dependence of fluorescence spectra of the native LHC II complex (blue dots connected with line). The uncertainty ranges are hidden by the data points.

4.3. Temperature shift in the absorption difference spectra of the LHC II mutants Chl *a*610, Chl *a*612 and Chl *b*606. Comparison with the protein dynamics of the native LHC II complex

The temperature dependence of the maxima of LHC II mutants Chl *a*610, Chl *a*612 and Chl *b*606 absorption difference spectra have been plotted in Figure 31 below.

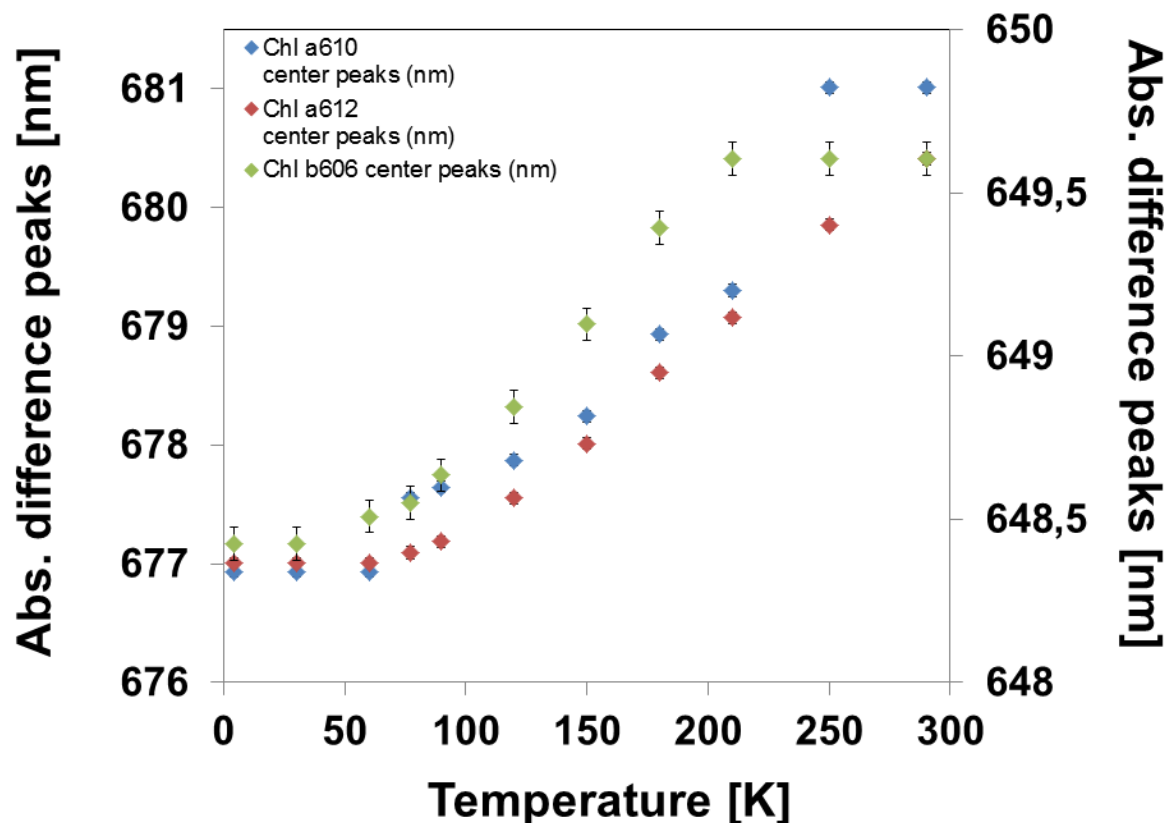
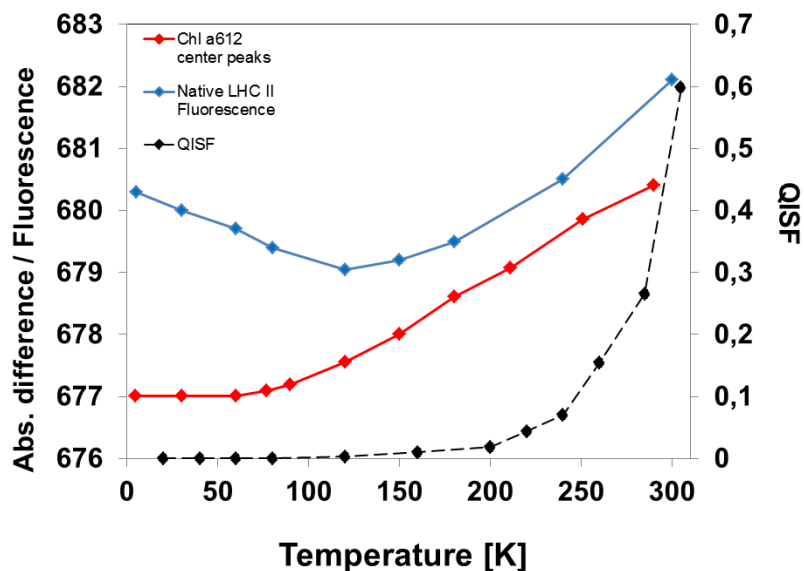


Figure 31: Temperature dependence of the maxima of LHC II mutants Chl *a*610 (blue points), Chl *a*612 (red points) and Chl *b*606 (green points) absorption difference spectra. Uncertainty ranges are given.

As it can be seen from Figure 31 and Figure 26, the maxima and FWHM values are first stable up to 77 K. After 77 K, the maximum point positions start shifting. In order to understand this shift better, protein dynamics of the native LHC II complex have been investigated using the QENS method. Maximum points of the LHC II mutant Chl *a*612 absorption difference spectra, the maximum points of the fluorescence spectra and the QENS spectra of the native LHC II complex are plotted as a function of temperature in Figure 32.

a)



b)

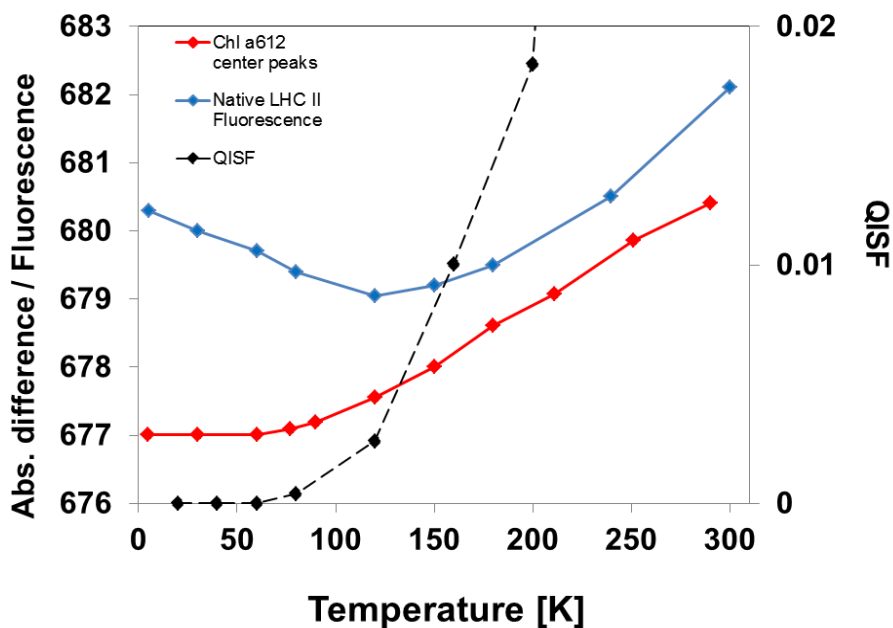


Figure 32: a) Temperature dependence of the maximum of LHC II mutant Chl *a*612 absorption difference spectra (red dots connected with line) compared to the temperature dependence of fluorescence spectra (blue dots connected with line) and QENS spectra (black dots connected with dashed line) of the native LHC II. The uncertainty ranges are hidden by the data points.

b) The QISF points from Figure a) have been magnified to emphasize the changes at 77 K.

In Figure 32 it can be seen that the maximum points of the LHC II mutant Chl *a*612 absorption difference spectra and the points of the QENS spectra of the native LHC II complex are first stable at lower temperatures up to 77 K. After the temperature reaches 77 K, the positions of the points start shifting.

The QENS data shows that conformational protein motions are frozen below 77 K. The protein motions get activated at 77 K and show a strong increase in protein flexibility with the dynamil transition at ~210 K. A similar temperature dependence, but at different transition temperatures, has been observed in Pieper et al. (2007) [22]. In their work, investigating the PS II membrane fragments, it has been revealed that protein motions are frozen below 120 K, activated after 120 K, and show the dynamic transition at 240 K.

It is remarkable that the QENS analysis reveals the same activation temperature for the protein motions as the temperature observed for the spectral position of the absorption bands above. This suggests a correlation of the two phenomena, and that the changes are not just structural but also dynamic. The peak positions of the absorption difference spectra of LHC II mutants are constant from 4.5 K up to 77 K, and then shift continuously. If there would be only structural changes, the peak positions would be constant before and after the structural transition.

A model for the potential energy diagram describing the coupling between protein dynamics and peak absorption wavelength of LHC II pigments will be presented in the next paragraph.

4.4. Potential energy diagram

The model of energy diagram in Figure 33 has two potential energy wells which reflect two different local conformations of the LHC II protein in the vicinity of Chl *a*612. With thermal activation excitation, meaning with the increase of temperature, the thermal population changes — but not the conformations. The QENS data presented above indicate that such thermally activated conformational protein motions occur in native LHC II above 77 K. If we increase the temperature enough, not only the lower well, but both wells will be populated. The higher the temperature, the likelier it is to find the system in the second state. If the first state is at 678 nm, and the second state is at 686 nm, and the system can switch between the two states, then the the system is at 678 nm at the low temperature. But with increasing temperature, the probability to find the system at 686 nm is increasing as well. The average peak position shifts continuously towards 682 nm, which is the average position of the two potential wells. And this explains the continuous shift. At low temperature, the peak positions are constant. The barrier between the two potential wells is so high

that the system cannot be found to the second (energetically higher) conformational state at all. But at higher temperatures there is a gradual increase of the probability for the system to be in the second conformational state.

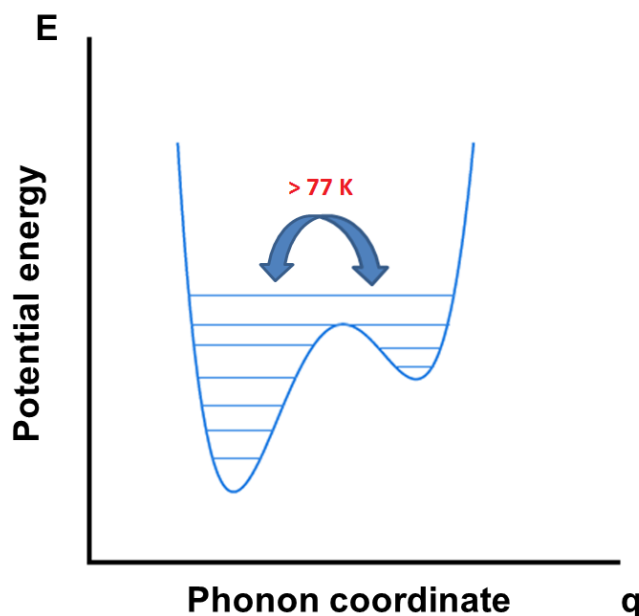


Figure 33: Potential energy diagram for LHC II.

4.5. Conclusions about the LHC II mutants Chl *a*610 and Chl *b*606

Chl *a*610 is the same strongly coupled Chl *a* trimer as Chl *a*612. Chl *a*610 has a more complex lineshape with three peak structures in its absorption spectrum. This is consistent with Chl *a*610 being part of an excitonically coupled Chl *a* trimer. We have no explanation why this structure is visible for Chl *a*610 but not for Chl *a*612, although these chlorophylls are excitonically coupled partners. Chl *a*612 appears as a single absorption band. The difference between *a*610 and *a*612 is currently an open research question. The temperature dependence of Chl *a*610 is affected by protein motions analogously to Chl *a*612.

Chl *b*606 contributes to the absorption at ~648 nm. And the fit of this absorption peak reveals Lorentzian broadening of 160 cm^{-1} that corresponds to a lifetime of 66 fs due to energy transfer. This value is probably overestimating the width, but this value still compares relatively well with the 100 fs component from the *b*606 to the *b*607 molecule according to the energy-level diagram (Figure 6) of van Grondelle and Novoderezhkin [14].

5. Summary

Light-harvesting complexes of plants play an important role in photosynthesis. They harvest solar energy and transfer it to the reaction center of a photosystem, where the energy conversion reactions are executed.

Energy transfer to the reaction center happens due to complex pigment-pigment and pigment-protein interactions. Even though structures of light-harvesting complexes have been revealed by the crystallographic methods, we still lack a complete understanding of the excitation energy transfer. The excitation energy transfer (EET) in photosynthetic light harvesting complexes occurs in femtoseconds, which makes it one of the fastest biological processes observed in nature.

Light-harvesting complex II (LHC II) is the most widespread and best studied pigment-protein complex. It serves as an antenna for the light-harvesting in green plants.

The main goal of this thesis is to analyze the effects of pigment-pigment interactions and protein dynamics at low and elevated temperatures by combining optical spectroscopy and quasielastic neutron scattering methods. This main goal has been achieved and the results of the analysis are summarized in the following.

During the data analysis, spectral positions and lineshapes of the three chlorophyll molecules have been determined from the mutants' absorption difference spectra in the temperature range 4.5 K – 290 K. It has been ascertained that Chl *a*612 contributes to fluorescence at all temperatures, but above 150 K Chl *a*612 becomes the main contributor.

The spectral position of the Chl *a*612 absorption band at ~677 nm exhibit a pronounced temperature dependence above 77 K all the way up to 680 nm. The temperature dependent shift appears to be correlated with thermally activated protein motions between different conformational substates that are thermally accessible above 77 K.

Chl *a*610 has a three peak structure in the absorption spectrum with peaks at ~670, ~672 and ~675 nm, because it is located in an excitonically coupled Chl *a* trimer. Chl *b*606 has a peak in the absorption band at ~648 nm. A fit of the absorption band reveals a Lorentzian lifetime broadening corresponding to a lifetime of 66 femtoseconds due to energy transfer.

S-factors in the three temperature ranges have been obtained from the analysis of absorption difference spectra of mutants. They are for Chl *a*612 0.44 at 4.5–60 K, 0.91 at 77—211 K; and 1.74 at 211—290 K; for Chl *a*610 0.45, 1.31, 1.05; and for Chl *b*606 0.47, 0.94, 1.82.

Quasielastic neutron scattering revealed three different temperature ranges with distinct protein dynamics: below 77 K, conformational protein motions are frozen. In the 77–240 K temperature range, protein motions are thermally activated. At temperatures higher than 240 K, protein motions are above the dynamical transition. Protein motions in these three temperature ranges differ in the magnitude of their dynamics.

It is remarkable that the QENS analysis reveals the same activation temperature for the protein motions as the temperature observed for the spectral position of the absorption bands above. This suggests a correlation of the two phenomena, and that the changes are not just structural but also dynamic.

Based on the analysis provided in this thesis it looks promising to analyze further LHC II mutants in order to understand the contributions of the different chlorophylls and gain a complete understanding of the inner working of the LHC II complex, and thus of photosynthesis itself. This will facilitate the design of new kind solar cell that absorbs light energy just as efficiently as nature does.

6. Summary in Estonian / Kokkuvõte

Taimede valgustneelavad kompleksid mängivad fotosünteesis tähtsat osa. Nad koguvad päikeseenergiat ja edastavad selle fotosüsteemi reaktsioonitsentrisse, kus toimuvad energiateisendusreaktsioonid.

Energiaülekanne reaktsioonitsentrisse toimub tänu keerukatele pigmentidevahelistele ning pigmentide ja proteiinide vahelistele reaktsioonidele. Ehkki valgustneelavate komplekside struktuure on kristallograafiliste meetoditega uuritud, ei mõista me ergastusenergia ülekandemehhanisme tänini täielikult. Ergastusenergia ülekanne (EET) fotosünteetilistes valgustneelavates kompleksides toimub femtosekundite jooksul, see on üks kiiremaid looduslikke bioloogilisi protsesse.

Valgustneelav kompleks II (LHC II) on levinuim ja enim uuritud pigmendi-proteini kompleks. Rohelistes taimedes toimib see valgustneelava antennina.

Käesoleva töö põhieesmärk on analüüsida pigmentidevaheliste reaktsioonide mõju ja proteiinide dünaamikat madalatel ja kõrgetel temperatuuridel, ühendades selektiivse optilise spektroskoopia ja kvaasielastse neutronhajumise meetodid. Põhieesmärk saavutati, järgnevas on esitatud analüüsitulemused.

Andmeanalüüsi vältel määrati kolme klorofüllimolekuli asendid spektris ja joonekujud mutantide neeldumisspektrite erinevuse alusel temperatuurivahemikus 4.5 K – 290 K. Tehti kindlaks, et Chl *a*612 osaleb fluorestseerumises iga temperatuuri juures, kuid ülalpool 150 K piiri annab Chl *a*612 sellesse põhipanuse.

Chl *a*612 neeldumisriba asendid spektris sõltuvad ülalpool 77 K selgelt temperatuurist. See korreleerub proteiinide termiliselt aktiveeritud liikumisega eri konformatsiooniliste seisundite vahel, mis 77 K-st kõrgemal termiliselt aktiveeruvad.

Chl *a*610 struktuur neeldumisspektris on kolmetipuline, kuna see paikneb paardunud eksitoniga Chl *a* trimeeris. Chl *b*606 neeldumisriba tipp asub ~648 nm juures. Neeldumisspekter näitab Lorentzi kontuurile vastavat laienemist, mis energiaülekande tõttu vastab 66 femtosekundi pikkusele elueale.

Mutantide neeldumisspektrite vahe analüüsist saadi kolme temperatuurivahemiku S-faktorid. Need on Chl *a*612 puhul 4.5–60 K juures 0.44, 77—211 K juures 0.91 ja 211—290 K juures 1.74; Chl *a*610 puhul 0.45, 1.31 ja 1.05; ning Chl *b*606 puhul 0.47, 0.94 ja 1.82.

Kvaasielastne neutronhajumine näitas kolme eripärase proteiinidünaamikaga temperatuurivahemikku: allpool 77 K konformatsiooniline proteiiniliikumine seiskub. 77–240 K vahel on proteiiniliikumine termiliselt aktiveerunud. Ülalpool 240 K jääb proteiinide liikumine dünaamilisest üleminekust kõrgemale. Proteiinide liikumine neis kolmes temperatuurivahemikus erineb nende dünaamika suurusjärgu poolest.

Käesolevas töös esitatud analüüsi põhjal näib olevat võimalik analüüsida teisiga LHC II mutante, et mõista eri klorofüllide osa LHC II kompleksi töös ning seeläbi ka fotosünteesis tervikuna. See aitab kaasa uut tüüpi päikesepatarei loomisele, mis neelaks valgusenergiat sama tõhusalt kui seda teeb loodus.

Acknowledgements

First and foremost I would like to thank my supervisor Prof. Jörg Pieper for helping me throughout my thesis and teaching me enormous amounts of interesting lessons with great patience. One could not wish for a better supervisor.

I would also like to thank all co-workers:

Laura Wilk in the laboratory of Prof. Werner Kühlbrandt at the Max-Planck-Institute Frankfurt, Germany, for preparation of the reconstituted LHC II and LHC II mutants.

Dr. Margus Rätsep in the laboratory of Prof. Arvi Freiberg at the University of Tartu for carrying out optical measurements together with Prof. Jörg Pieper.

My supervisor Prof. Jörg Pieper for carrying out the optical and QENS measurements.

I would like to thank also the managers of my master's program, Prof. Ivo Leito and Sergei Jurtšenko, for creating and administering the program.

I would like to thank all my coursemates for making my study time in Tartu interesting.

Finally, I would like to thank my family and especially my dear husband for unconditional support throughout my studies in Tartu.

Research was supported by Estonian Research Council (Grant ETF 9453).

References

1. G. S. Singhal, G. Renger, S. K. Sopory, K. D. Irrgang, Govindjee, Concepts in Photobiology: Photosynthesis and Photomorphogenesis, Narosa Publishers/New Delhi, and Kluwer Academic/Dordrecht, 1999, pp. 11–51.
2. J. Austin, L. Staehelin, Three-Dimensional Architecture of Grana and Stroma Thylakoids of Higher Plants as Determined by Electron Tomography, *Plant Physiol.* 155 (2011), 1601–1611.
3. J. Mahendra, Photosynthesis, *Competition Science Vision* 61 (2003) 103–105.
4. D. Richfield, Chemical structures of Chl *a* and Chl *b*. Images from:
http://commons.wikimedia.org/wiki/File:Chlorophyll_a.svg accessed 28.02.2013.
http://commons.wikimedia.org/wiki/File:Chlorophyll_b.svg accessed 28.02.2013.
5. M. Johnson, T. Goral, C. Duffy, A. Brain, C. Mullineaux, A. Ruban, Photoprotective Energy Dissipation Involves the Reorganization of Photosystem II Light-Harvesting Complexes in the Grana Membranes of Spinach Chloroplasts, *The Plant Cell* April 4 (2011) 1468–1479.
6. J. Pieper, Application of high-resolution spectroscopy investigating the energy level structure and electron-phonon coupling of the light-harvesting complex II of green plants, Dissertation, Humboldt University of Berlin, 2000, pp. 1–143.
7. Z. Liu, H. Yan, K. Wang, T. Kuang, J. Zhang, L. Gui, X. An, W. Chang, Crystal structure of spinach major light-harvesting complex at 2.72 Å resolution, *Nature* 428 (2004), 287–292.
8. A. Nilsson, D. Stys, T. Drakenberg, M. Spangfort, S. Forsén, J. Allen, Phosphorylation controls the three-dimensional structure of plant light harvesting complex II, *J. Biol. Chem.* 272 (1997) 18350–18357.
9. W. Kühlbrandt, D. Wang, Y. Fujiyoshi, Atomic model of plant light-harvesting complex by electron crystallography, *Nature* 367 (1994), 614–621.
10. J. Standfuss, A. van Scheltinga, M. Lamborghini, W. Kühlbrandt, Mechanisms of photoprotection and nonphotochemical quenching in pea light-harvesting complex at 2.5 Å resolution, *EMBO J.* 24 (2005), 919–928.
11. K. Irrgang, E. Boekema, J. Vater, G. Renger, Structural determination of the Photosystem II core complex from spinach. *Eur. J. Biochem.* 178 (1988), 209–217.
12. H. Lichtenthaler, *Methods Enzymol.* 148 (1987) 350–382.
13. H. Rogl, R. Schödel, H. Lokstein, W. Kühlbrandt, A. Schubert, Assignment of spectral

- substructures to pigment-binding sites in higher plant light-harvesting complex LHC-II, *Biochem. 41* (2002), 2281–2287.
14. R. van Grondelle, V. Novoderezhkin, Energy transfer in photosynthesis: experimental insights and quantitative models, *Phys. Chem. Chem. Phys. 8* (2006), 793–807.
 15. McGraw-Hill Dictionary of Scientific and Technical Terms (6th edition), McGraw-Hill Professional, 2002, pp. 1–2380.
 16. J. Pieper, A. Freiberg, Electron-phonon and exciton-phonon coupling in light-harvesting, insights from line-narrowing spectroscopies, Book chapter, In press.
 17. G. Kneller, Quasielastic Neutron Scattering, Lecture B9, Hercules (2004), 5.
 18. J. Wuttke, Scheme of inelastic neutron scattering experiment. Image from:
<http://upload.wikimedia.org/wikipedia/en/5/51/Inelastic-neutron-scattering-basics.png> accessed 13.04.2013.
 19. J. Pieper, G. Renger, Protein dynamics investigated by neutron scattering, *Photosynth. Res. 102* (2009), 281–293.
 20. European Spallation Source: <http://europeanspallationsource.se/> accessed 13.04.2013
 21. M. Marconi, A. de Francesco, E. Cornicchi, G. Onori, A. Paciaroni, Hydration and temperature dependent dynamics of lysozyme in glucose-water matrices. A neutron scattering study, *Chem. Phys. 317* (2005), 274–281.
 22. J. Pieper, T. Hauß, A. Buchsteiner, K. Baczynski, K. Adamiak, RE. Lechner, Temperature- and hydration-dependent protein dynamics in photosystem II of green plants studied by quasielastic neutron scattering, *Biochem. 46* (2007), 11398–11409.
 23. A. Gall, J. Seguin, B. Robert, M-C. Bellissent-Funel, Membrane proteins in bulk solution can be Used for quasielastic neutron scattering studies: the case for the photochemical reaction center, *J. Phys. Chem. 106* (2004), 6303–6309.
 24. S. Combet, J. Pieper, F. Coneggio, J-P. Ambroise, M-C. Bellissent-Funel, J-M. Zanotti, Coupling of laser excitation and inelastic neutron scattering: attempt to probe the dynamics of light-induced C-phycoyanin dynamics, *Eur. Biophys. J. 37* (2008) 693.
 25. J. Pieper, K-D. Irrgang, G. Renger, RE. Lechner, Density of vibrational states of the light-harvesting complex II of green plants studied by inelastic neutron scattering, *J. Phys. Chem. 108* (2004), 10556–10565.
 26. J. Pieper, T. Hauß, A. Buchsteiner, G. Renger, The effect of hydration on protein flexibility in photosystem II of green plants studied by quasielastic neutron scattering, *Eur. Biophys. J. 37*

- (2008) 657–663.
27. E. Peterman, S. Hobe, F. Calkoen, R. van Grondelle, H. Paulsen, H. van Amerongen, Low-temperature spectroscopy of monomeric and trimeric forms of reconstituted light-harvesting chlorophyll a/b complex, *Biochim. Biophys. Acta* 1273 (1996) 171–174.
 28. H. Rogl, W. Kühlbrandt, Mutant trimers of light-harvesting complex II exhibit altered pigment content and spectroscopic features, *Biochemistry* 38 (1999) 16214–16222.
 29. R. Lechner, Optimization of the chopper system for the cold-neutron time-of-flight spectrometer NEAT at the HMI-Berlin, *Physica B* 180–181 (1992) 973–977.
 30. R. Azuah, L. Kneller, Y. Qiu, P. Tregenna-Piggott, C. Brown, J. Copley, R. Dimeo, DAVE: a comprehensive software suite for the reduction, visualization, and analysis of low energy neutron spectroscopic data, *J. Res. Natl. Inst. Stan. Technol.* 114 (2009) 341–358.
 31. J. Pieper, J. Voigt, G. Renger, G. Small, Analysis of phonon structure in line-narrowed optical spectra, *Chemical Physics Letters* 310 (1999), 296–302.
 32. <http://www.wolfram.com/mathematica/> accessed 28.05.2013.
 33. E. Belgio, A. Casazza, G. Zucchelli, F. Garlaschi, R. Jennings, Band shape heterogeneity of the low-energy chlorophylls of CP29: absence of mixed binding sites and excitonic interactions, *Biochemistry* 49 (2010), 882–892.

Non-exclusive licence to reproduce thesis and make thesis public

I, Kamarniso Vrandecic

(author's name)

(date of birth: 20.11.1989),

1. herewith grant the University of Tartu a free permit (non-exclusive licence) to:

1.1. reproduce, for the purpose of preservation and making available to the public, including for addition to the DSpace digital archives until expiry of the term of validity of the copyright, and

1.2. make available to the public via the web environment of the University of Tartu, including via the DSpace digital archives until expiry of the term of validity of the copyright,

Energy level structure and protein dynamics in the light-harvesting complex II,

(title of thesis)

supervised by Prof. Jörg Pieper,

(supervisor's name)

2. I am aware of the fact that the author retains these rights.

3. I certify that granting the non-exclusive licence does not infringe the intellectual property rights or rights arising from the Personal Data Protection Act.

Tartu, 03.06.2013 (date)